

A Radically New Theory of how the Brain Represents and Computes with Probabilities

Rod Rinkus, Neurithmic Systems & Volen Center for Complex Systems, Brandeis University

Abstract

It is widely acknowledged that the brain i) implements probabilistic reasoning, and ii) represents information via population/distributed coding. Most previous population-based probabilistic (PPC) theories share several basic properties: 1) continuous (graded) neurons; 2) fully/densely-distributed coding, i.e., all/most coding field neurons formally participate in every code; 3) graded synapses; 4) rate coding; individual neurons are assumed to 5) have unimodal, e.g., bell-shaped, tuning functions (TFs) and 6) be fundamentally noisy; and 7) noise/correlation are generally viewed as problems requiring mitigation. In contrast, our theory assumes: 1) binary neurons; 2) only a small subset of neurons, i.e., a *sparse distributed code* (SDC), comprises any individual code; 3) binary synapses; 4) signaling formally requires only single, i.e., first, spikes; individual neurons 5) initially have completely flat TFs (all weights zero) and 6) are not noisy; and 7) noise is a resource generated and used to achieve the crucial property that more similar inputs map to more similar codes, which controls a tradeoff between storage capacity and embedding the statistics of the input space in the pattern of intersections over the codes, indirectly yielding particular correlation patterns. The theory, Sparsey, was introduced 20 years ago as a canonical cortical circuit/algorithm model, but its interpretation as a probabilistic model was not emphasized. Sparsey's efficient similarity preserving mechanism yields fixed-time learning and best-match retrieval (inference), i.e., time independent of the number of stored hypotheses (memories). Assuming input similarity correlates with likelihood, which is quite reasonable over large regions of natural input spaces, the active SDC code simultaneously represents both the most probable hypothesis and the probability distribution over all stored hypotheses. We show this for spatial and spatiotemporal (sequential) cases. In the latter case, the entire distribution is updated, on each sequence item, in fixed time. Finally, consistent with moving beyond the Neuron Doctrine to the view that the SDC (cell assembly, ensemble) is the fundamental neural unit of representation/thought, Sparsey suggests that classical unimodal TFs emerge as an artifact of a single/few-trial learning process in which SDC codes are laid down in superposition.

Keywords

Sparse distributed codes, sparse distributed representations, probabilistic population coding, locality-sensitive hashing, learning hashing, cell assemblies, ensemble coding, combinatorial code, sequence recognition, sparse distributed memory, neural noise, neural correlation, recurrent neural net, episodic memory, associative memory, canonical cortical circuit, macrocolumn, minicolumn

Introduction

It is widely acknowledged that the brain must implement some form of probabilistic reasoning to deal with uncertainty in the world (Pouget, Beck et al. 2013). However, exactly how the brain represents probabilities/likelihoods remains unknown (Ma and Jazayeri 2014, Pitkow and angelaki 2016). It is also widely agreed that the brain represents information with some form of distributed—a.k.a. population, cell-assembly, ensemble—code [see (Barth and Poulet 2012) for relevant review]. Several population-based probabilistic coding theories (PPC) have been put forth in recent decades, including those in which the state of all neurons comprising the population, i.e., the *population code*, is viewed as representing: a) the single

most likely/probable input value/feature (Georgopoulos, Kalaska et al. 1982); or b) the entire probability/likelihood distribution over features (Zemel, Dayan et al. 1998, Pouget, Dayan et al. 2000, Pouget, Dayan et al. 2003, Jazayeri and Movshon 2006, Ma, Beck et al. 2006, Boerlin and Denève 2011). Despite their differences, these approaches share fundamental properties, a notable exception being the spike-based model of (Boerlin and Denève 2011).

1. Neural activation is continuous (graded).
2. *All* neurons in the coding field formally participate in the active code whether it represents a single hypothesis or a distribution over all hypotheses. Such a representation is referred to as a *fully distributed* representation.
3. Synapse strength is continuous (graded).
4. These approaches have generally been formulated in terms of rate-coding (Sanger 2003), which requires significant time, e.g., order 100 ms, for reliable decoding.
5. They assume *a priori* that the tuning functions (TFs) of the neurons are unimodal, bell-shaped over single dimensions, and consequently do not explain how such TFs might develop through learning.
6. Individual neurons are assumed to be noisy, e.g., firing with Poisson variability.
7. Noise and correlation are viewed primarily as problems that have to be dealt with, e.g., reducing noise correlation by averaging.

At a deeper level, it is clear that despite being framed as population models, they are really based on an underlying localist interpretation, specifically, that an individual neuron's firing rate can be taken as a perhaps noisy estimate of the probability that a single preferred feature (or preferred value of a feature) is present in its receptive field (Barlow 1972). While these models entail some method of combining the outputs of individual neurons, e.g., voting or averaging, each neuron is viewed as providing its own individual estimate of the input feature, i.e., each neuron possesses its own independent (typically bell-shaped) TF, or *encoding model* (Deneve and Chalk 2016). For example, this can be seen quite clearly in Figure 1 of (Jazayeri and Movshon 2006) wherein the first layer cells (sensory neurons) are unimodal and therefore can be viewed as detectors of the value at their modes (preferred stimulus) and the *pooling* cells are also in 1-to-1 correspondence with directions. This is a localist representation has the limitation that the maximum number of features (or individual feature values), e.g., directions, that can be stored, i.e., the storage capacity, equals the number of pooling cells. This underlying localist interpretation is present in the other PPC models referenced above as well.

The theory described herein, Sparsey, constitutes a radically new way of representing and computing with probabilities in which:

1. The neurons comprising the coding field need only be *binary*.
2. Individual represented hypotheses are represented by fixed-size, sparsely chosen subsets of the population, i.e., a *sparse distributed codes* (SDC) (Rinkus 1996, Rinkus 2014).
3. Decoding (read-out) of the most likely hypothesis and of the entire distribution by downstream computations, requires only binary synapses.
4. Signaling can be communicated via waves of contemporaneously arriving first-spikes (e.g., within a few ms window, likely organized by local gamma) from afferent SDC codes to downstream

computations (including recurrently to the source coding field), thus in principal, 1-2 orders of magnitude faster than rate coding.. Thus, signaling formally requires only single, i.e., first, spikes, meaning that Sparsey is not essentially a spiking model, though of course spikes are the brain's currency.

5. The initial weights of all afferent synapses to all neurons comprising the field are zero, i.e., the TFs are completely flat. Roughly unimodal TFs [as would be revealed by low-complexity probes, e.g., oriented bars spanning a cell's receptive field (RF)] emerge as a side-effect of the model's single/few-trial learning process of laying down SDCs in superposition *if the process of choosing those SDCs preserves similarity*.
6. Neural activation is not noisy. Individual neurons are simply on or off on any given computational cycle. We make no use of precise spike times, but assume that some meta-circuitry organizes (temporally collects) transmission of *en masse* synaptic signals from an SDC coding field within some small window of arrival at a downstream decoding field. Our working assumption is that this is the purpose of the gamma cycle (Fries 2009, Buzsáki 2010, Igarashi, Lu et al. 2014, Watrous, Fell et al. 2015).
7. Noise, is viewed essentially as a resource. It is explicitly generated and injected into the code selection process to achieve a specific coding goal, namely that the overall set of codes stored in a coding field has the property that similar inputs map to similar codes ("SISC"). This has straightforward implications on correlation, described below.

SDC admits a completely different concept for representing and computing with probabilities than is possible under either localist or fully distributed representations. In SDC, instead of representing a feature, X, by the state of a *single* neuron, it is represented by a *set* of neurons, specifically, a small subset of the whole coding field, which we refer to as X's code. All neurons participating in the code are fully active and the rest of the coding field's neurons are completely off. Thus:

- A. Gradations in the certainty, or probability, that X is present in the receptive field (RF) of the SDC coding field (population) can be represented by different *fractions* of X's code being active.
- B. Communication of X's probability to target (downstream, or subsequent) computations—i.e., *decoding*—can be achieved by neurons participating in such target computations simply *summing* their binary synaptic inputs from the field in which X is active.

Thus, representing and using graded values, e.g., probabilities, requires only binary neurons and binary synapses. There is no need for explicit *localist* representation of graded values, anywhere in the system/computation. More specifically, there is no need to represent probabilities/likelihoods localistically in the form of firing rates and there is no need to represent conditional probabilities, or strengths of association, via continuous/graded weights. Moreover, although neurons presumably communicate primarily via spikes, conceiving the signal sent from an active SDC code as a vector of contemporaneously arriving first spikes (to a target field) essentially removes the need to cast our treatment in terms of a "spiking model" with its assumed (typically Poisson) intrinsic noisiness. Rather, our approach has more the character of an algorithm operating according to a discrete clock (whose basic cycle, we suppose to correspond to a gamma cycle). Thus, our approach does not assume intrinsic noise 'that has to be dealt with', but rather injects a state-dependent amount of noise (or inversely, correlation), by manipulating neurons' transfer functions, to achieve certain coding goals, as discussed below.

The unique property of sparse distributed coding that it allows the similarity of represented features to be represented by the intersection size of their codes, i.e., SISC, has been pointed out in the past (Rinkus 1996, Rachkovskij and Kussul 2001, Kanerva 2009). However, the possibility of:

- a) interpreting the fraction of a feature’s SDC code that is active as the probability/likelihood of that feature (hypothesis), and
- b) interpreting the code active in an SDC coding field, whether it be a reactivation of a previously stored code or a novel code (which nevertheless, may generally overlap with many previously stored codes), as a *distribution over all codes (and thus, over all represented features) stored in the field*

was introduced in (Rinkus 2012). Similarity preservation, involving a continuous measure, e.g., Euclidean distance, has also been established for fully distributed coding models, e.g., (Bogacz 2007). However, such codes have not been interpreted as *simultaneously* representing *both* the most likely hypothesis and the entire distribution and in any case, as noted above, in such models, decoding by downstream computations requires either graded synapses or rate-coding.

Above, we refer to the “RF of the SDC coding field” rather than to the RF of an individual neuron. This is because we require that, to first approximation, all neurons in the SDC coding field have the same RF in order to assert that the codes in that field represent features present in the RF. This constraint can be relaxed to some extent, but it facilitates initial exposition and analysis. In any case, this constraint actually serves to further underscore the massive gulf between Sparsey and previous PPC theories for which this constraint is not needed, even approximately, due to their underlying localist conception. Sparsey evinces a new paradigm of neuroscience in which the ensemble (SDC, cell assembly), not the single neuron, is considered the fundamental functional unit, i.e. a move away from the ‘Neuron Doctrine’ as for example, advocated in (Yuste 2015, Fusi, Miller et al. 2016, Schneidman 2016). We expect that with rapidly advancing methods [recent reviews: (Hamel, Grewe et al. 2015, Jercog, Rogerson et al. 2016)] allowing observation of the activities of all neurons in substantial (e.g., order hypercolumn/barrel-sized) volumes and with progressively smaller temporal precision, issues such as our connectivity assumption will be addressable.

In the results section, we present two simulation-backed examples showing the mechanistic details of how Sparsey’s core algorithm, the *code selection algorithm* (CSA) (Rinkus 1996, Rinkus 2004, Rinkus and Lisman 2005, Rinkus 2008, Rinkus 2010, Rinkus 2013, Rinkus 2014), activates not only the code of the best-matching, or most likely, input, but also activates the similarity/likelihood distribution over *all* stored inputs. Moreover, the CSA accomplishes this with a number of steps that remains constant as the number of stored inputs increases, a property that we call *fixed* time complexity. The first example shows this for the case of purely spatial inputs. The second example shows that when the coding field is recurrently connected, the entire distribution is updated from time T to T+1 [which can be viewed as *belief update* (Pearl 1988)] in a way that is consistent with the statistics of the domain, again, in *fixed* time. Moreover, as explained previously (Rinkus 2010, Rinkus 2014), the CSA also stores, or learns, new inputs, spatial or spatiotemporal, in fixed time. In fact, Sparsey/CSA can be viewed as a hashing method which learns a locality-sensitive, i.e., similarity-preserving, hash function from the data (which can be spatial or spatiotemporal). While other neurally inspired hashing models have fixed-time best-match retrieval (Salakhutdinov and Hinton 2007, Salakhutdinov and Hinton 2009, Grauman and Fergus 2013), they do not also have fixed-time learning. In fact, none of the currently state-of-art hashing models described in a recent review (Wang, Liu et al. 2016) possess both fixed-time learning and fixed-time best-match retrieval. Although time complexity considerations like these have generally not been discussed in the probabilistic

population coding literature, they are essential for evaluating the overall plausibility of models of biological cognition, for while it is uncontroversial that the brain computes probabilistically, we also need to explain the extreme speed with which these computations, which are over potentially quite large hypothesis spaces, occur.

A crucial reason why Sparsey achieves fixed time performance for both learning and best-match retrieval is its unique and simple method for computing the *global familiarity*, G , of an input and using it to control the selection of a code for that input. By ‘global’, we mean that G is a function of all cells comprising the coding field, in contrast to *local familiarity*, V_i , which is cell i ’s local (depending only on its synaptic inputs) measure of its match to the input. Crucially, computing G *does not require* explicitly comparing the new input to every stored input (nor to a log number of the stored inputs as is the case for tree-based methods). Rather, the G computation, whose time complexity is dominated by a single pass over the *fixed* number of afferent weights to the field, implicitly performs these comparisons simultaneously, in an algorithmically parallel fashion. ‘Algorithmic parallelism’ means that single atomic operations affect multiple represented (stored) items. Thus, operationally, ‘algorithmic parallelism’ is very close if not identical to ‘distributed representation’: you cannot have one without the other. We emphasize that algorithmic parallelism and machine parallelism are orthogonal resources and are fully compatible.

In most prior SDC models, the coding field is a homogenous field of binary units from which some number are chosen to be in any particular code (Kanerva 1988, Rachkovskij and Kussul 2001, Hecht-Nielsen 2007, Snaider and Franklin 2011, Snaider and Franklin 2012, Snaider and Franklin 2012, Snaider and Franklin 2014, Ahmad and Hawkins 2015, Cui, Ahmad et al. 2016). This is also true of *combinatorial neural codes* (Willshaw, Buneman et al. 1969, Curto, Itskov et al. 2013) as well as for all the binary hashing models reviewed in (Wang, Liu et al. 2016). In contrast, in Sparsey, the coding field consists of Q winner-take-all (WTA) competitive modules (CMs), each comprised of K binary units. Selecting a code is performed by making an independent draw in each of the Q CMs. Thus, unlike these other homogenous-field models, Sparsey has an explicit structural mesoscale, the WTA CM, situated between single neuron and the whole coding field. In fact, from its inception, Sparsey has been offered as a generic model of the cortical macrocolumn, with its WTA CMs proposed as analogous to minicolumns (Rinkus 1996, Rinkus 2010, Rinkus 2014). We therefore use “coding field” and “macrocolumn”, or just, “mac”, interchangeably, throughout this paper.

A simplified version of the CSA, sufficient for this paper’s examples, is given in Table 1, but we briefly summarize it here. CSA Step 1 computes the input sums for all $Q \times K$ cells comprising the coding field. Specifically, for each cell, a separate sum is computed for each of its major afferent synaptic projections, e.g., bottom-up (U), horizontal (H), and top-down (D) projections, the latter two of which provide recurrence to the coding field. This is the step requiring the aforementioned single pass over the field’s afferent weights. In Step 2, these sums are normalized and in Step 3, the normalized sums are (optionally nonlinearly transformed and) multiplied, yielding the V values. In Steps 4 and 5, G is computed as the average max V across the Q CMs. In the remaining CSA steps, G is used, in each CM, to nonlinearly transform the V distribution over the K cells into a final ρ distribution from which a winner is picked. G ’s influence on the distributions can be summarized as follows.

- a) When high global familiarity is detected ($G \approx 1$), those distributions are exaggerated to bias the choice in favor of cells that have high input summations, and thus, high *local* familiarities, V_i , which acts to increase correlation.

- b) When low global familiarity is detected ($G \approx 0$), those distributions are flattened so as to reduce bias due to local familiarity, which acts to increase the expected Hamming distance between the selected code and previously stored codes, i.e., to decrease correlation.

Since the V values represent *signal*, exaggerating the V distribution in a CM multiplicatively (as is achieved via CSA Eqs. 6-8) increases signal and flattening it increases noise. The above behavior (and its smooth interpolation over the range, $G=1$ to $G=0$) is the means by which Sparsey achieves SISC. And, it is the enforcement (statistically) of SISC during learning, which ultimately makes possible the immediate (fixed time complexity) retrieval of the best-matching (or most likely, most relevant) hypothesis and the simultaneous fixed-time update of *all* stored hypotheses (i.e., via algorithmic parallelism, not machine parallelism) with each new input.

Novel explanation of noise and correlation

In recent years, there has been much discussion about the nature, causes, and uses, of correlations and noise in cortical activity; see (Kohn, Coen-Cagli et al. 2016), Schneidman (2016) for reviews. Most investigations of neural correlation and noise, especially in the context of PPC theories, assume *a priori*: a) fundamentally noisy neurons, e.g., Poisson spiking; and b) tuning functions (TFs) of some general form, e.g., unimodal, bell-shaped, and then describe how noise/correlation affects the coding accuracy of populations with such TFs (Abbott and Dayan 1999, Moreno-Bote, Beck et al. 2014, Franke, Fiscella et al. 2016, Rosenbaum, Smith et al. 2017). Specifically, these treatments measure correlation of spiking rates. However, as noted above, our theory makes neither assumption. In our theory, the correlation of two neurons increases to the extent that they co-occur across multiple SDC codes. And, as noted at the outset, our theory assumes all afferent weights to the coding field are initially zero. i.e., the TFs are completely flat. Our theory explains how noise is actively controlled *during the learning process* so as to achieve certain goals regarding the set of SDC codes ultimately stored in the coding field. Both single-cell TFs and indirectly, particular patterns of correlation, emerge as side-effects of cells being selected to participate in such codes. The overarching goal is simply to enforce SISC. However, enforcing SISC in the context of an SDC coding field realizes a balance between:

- a) maximizing the storage capacity of the coding field, and
- b) embedding the similarity structure of the input space in the set of stored codes, which in turn enables fixed-time best-match retrieval.

Interestingly, in exploring the implications of shifting focus from information theory to coding theory in terms of influence upon theoretical neuroscience, (Curto, Itskov et al. 2013) have pointed to this same tradeoff, though their treatment uses error rate (coding accuracy) instead of storage capacity. We point out that understanding how neural correlation ultimately affects things like storage capacity is considered largely unknown and an active area of research (Latham 2017).

Classical Neural Tuning Functions as Artifacts

Neurons have classically been considered noisy because of high firing variability across presentations of the same stimuli. However, the difficulty of ensuring that stimuli are truly “the same” across trials is widely understood. Improving experimental methods have engendered an emerging view that the TFs of individual cells are much more heterogeneous than previously thought, e.g., having multiple modes (Cox and DiCarlo 2008, Bonin, Histed et al. 2011, Mante, Sussillo et al. 2013, Nandy, Sharpee et al. 2013, Nandy, Mitchell et al. 2016), also described as having “mixed selectivity” (Fusi, Miller et al. 2016). And, modeling complex/irregular TFs more precisely minimizes the variation that needs to be accounted for as noise. Sparsey embraces this more modern view in that the TFs of individual cells, which emerge over the course

of learning, are far less regular than the classical, unimodal, bell-shaped TFs and idiosyncratic to the specific inputs in whose codes they participated. Yet, because Sparsey preserves input similarity into the code space (i.e., SISC property), a more regular (lower complexity) structure can be seen when the set of inputs in whose codes a given cell has participated are averaged, i.e., in the reverse correlations of individual cells. The final section of the Results provides semi-quantitative support for this, suggesting the possibility that the archetypical, unimodal, bell-shaped, single-cell TFs that have been observed for 60+ years are simply artifacts of the underlying SDC-based learning/retrieval operations of the brain.

Results

A Single SDC Code Represents an Entire Similarity/Probability Distribution: Conceptual Introduction

Figure 1a shows the particular SDC format used in this paper. The coding field consists of Q winner-take-all (WTA) competitive modules (CMs), each consisting of K binary neurons. Here, $Q=7$ and $K=7$. Thus, all codes have exactly Q active neurons and there are K^Q possible codes. We assume that the input field of binary neurons (hexagons), e.g., representing an 8x8 pixel patch of visual field, is completely connected to the coding field (blue lines represent weights). All weights are initially zero. Figure 1b shows a particular input A , which has been associated with a particular code, $\phi(A)$; here, blue lines indicate the weights that would be increased from 0 to 1 to store this association (memory trace).

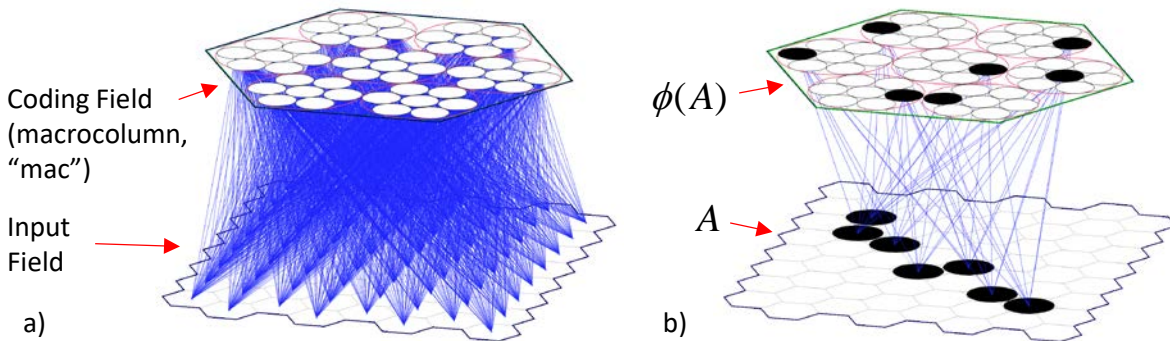


Figure 1: a) The sparse distributed coding field (macrocolumn, “mac”) consists of $Q=7$ WTA competitive modules. An input field of binary neurons is completely connected to the coding field. b) A particular input A , its code, $\phi(A)$, consisting of Q active (black) neurons, and the weights that would be increased to form the association are shown.

Figure 2 shows how the strength of presence, i.e., probability or likelihood, of a feature in the coding field’s RF is represented in our SDC-based theory. The figure shows five hypothetical inputs, A-E, which have been learned, i.e., associated with codes, $\phi(A)$ - $\phi(E)$. We hand-chose these particular codes to be consistent with the principle that similar inputs should map to similar codes (SISC). That is, inputs B to E have progressively smaller overlaps with A and therefore codes $\phi(B)$ to $\phi(E)$ have progressively smaller intersections with $\phi(A)$. The CSA has been shown to statistically enforce SISC for both the spatial and spatiotemporal (sequential) input domains (Rinkus 1996, Rinkus 2008, Rinkus 2010, Rinkus 2013, Rinkus 2014). For input spaces for which it is plausible to assume that input similarity correlates with likelihood, the single active code can therefore also be viewed as a probability distribution over all stored codes. As shown in the leftmost panel at the bottom of Figure 2, when $\phi(A)$ is 100% active, the other codes are partially active in proportions that reflect the similarities of their corresponding inputs to A, and thus, their

probabilities, i.e., the likelihoods of the inputs they represent. The remaining four panels show input similarity (likelihood) approximately correlating with code overlap.

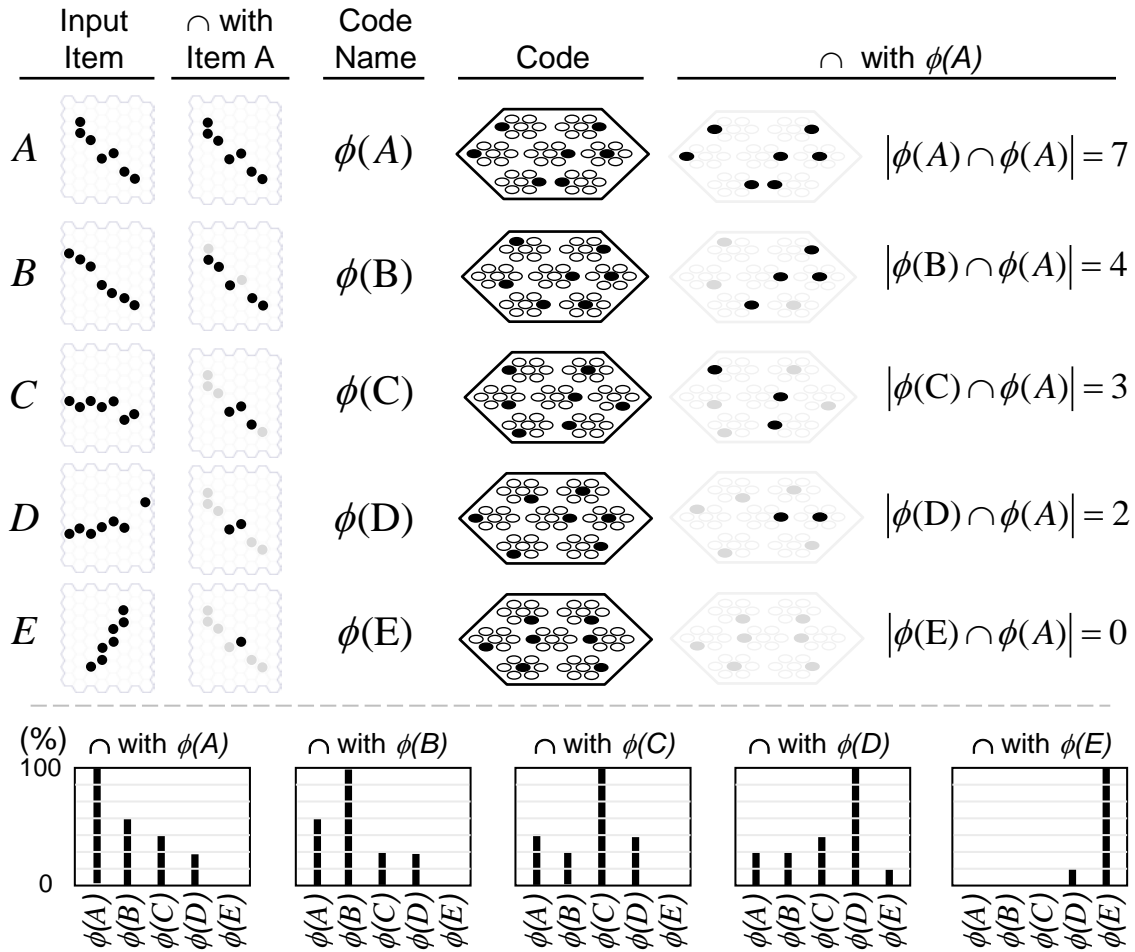


Figure 2: Illustration of how the probability/likelihood of a feature can be represented by the fraction of its code that is active. When $\phi(A)$ is fully active, the hypothesis that feature A is present can be considered maximally probable. Because the similarities of the other features to the most likely feature, A, correlate with their codes' overlaps with $\phi(A)$, the likelihoods of those features are represented by the fraction of their codes that are active. In the intersection (" \cap ") columns, black indicates units intersecting with either the input pattern A or its code, $\phi(A)$; gray indicates non-intersecting units.

The example of Figure 2 was constructed to illustrate the desired property that the similarities, and thus, likelihoods, of all stored hypotheses are simultaneously physically active whenever any single hypothesis is fully active. The next section demonstrates that the CSA achieves this property for purely spatial inputs and the following section, for the spatiotemporal case. Table 1 presents a simplified version of the code selection algorithm (CSA) with the minimal steps needed for these demonstrations. Specifically: a) we use a model with only one internal level, thus there are no D signals; b) all spatial inputs have exactly 12 active pixels, thus the U normalizer can be constant, $\pi_U = 12$; and c) the internal level consists of a single coding field (mac), thus the H normalizer can be constant, $\pi_H = Q - 1$.

Table 1: Simplified CSA

	Equation	Short Description
1	$u(i) = \sum_{j \in \text{RF}_U} x(j)w(j,i)$ $h(i) = \sum_{j \in \text{RF}_H} x(j,t-1)w(j,i)$	Compute raw U (and H, if applicable) input sums.
2	$U(i) = u(i)/\pi_U w_{\max}$ $H(i) = h(i)/\pi_H w_{\max}$	Compute normalized U (and H, if applicable) input sums. In this paper's simulations, $\pi_U = 12$ and $\pi_H = Q - 1$.
3	$V(i) = \begin{cases} H(i)^{\lambda_H} U(i)^{\lambda_U} & t \geq 1 \\ U(i)^{\lambda_U} & t = 0 \end{cases}$	Compute local evidential support for each cell. In this paper, $\lambda_H = \lambda_U = 1$, unless otherwise stated.
4	$\hat{V}_j = \max_{i \in C_j} \{V(i)\}$	Find the max V , \hat{V}_j , in each CM, C_j
5	$G = \sum_{q=1}^Q \hat{V}_q / Q$	Compute G as average \hat{V} value over the Q CMs
6	$\eta = 1 + \left(\left[\frac{G - G^-}{1 - G^-} \right]^+ \right)^\gamma \times \chi \times K$	Determine expansivity (η) of V -to- η sigmoid function. In this paper, $\gamma=2$, $\chi=100$, $G^- = 0.1$
7	$\sigma_1 = \frac{((\eta - 1)/0.001)^{1/\sigma_4} - 1}{e^{\sigma_2 \sigma_3}}$	Sets σ_1 so that the overall sigmoid shape is preserved over full η range. $\sigma_2 = 7.0, \sigma_3 = 0.4, \sigma_4 = 9.5$
8	$\psi(i) = \frac{(\eta - 1)}{(1 + \sigma_1 e^{-\sigma_2 (V(i) - \sigma_3)})^{\sigma_4}} + 1$	To each cell, apply sigmoid function, which collapses to constant fn, $\psi(i) = 1$, when $G \leq G^-$
9	$\rho(i) = \frac{\psi(i)}{\sum_{k \in \text{CM}} \psi(k)}$	In each CM, normalize relative (ψ) to final (ρ) probabilities of winning
10		Select a final winner in each CM according to the ρ distribution in that CM, i.e., soft max.

Single SDC Code Represents Entire Probability Distribution: Spatial Case

Figure 3a shows six inputs, I_1 to I_6 (which are disjoint for simplicity of exposition) that have been previously stored in the model instance depicted in Figure 3b. The model has a 12x12 binary pixel input level that is completely connected to all cells comprising the mac. The mac consists of $Q=24$ WTA CMs, each having $K=8$ binary cells. The second row of Figure 3a shows a novel test stimulus, I_7 , and its varying overlaps (red pixels) with I_1 to I_6 . Given that all inputs have exactly 12 active pixels, we can measure spatial similarity simply as size of intersection divided by 12 (shown as decimals under inputs):

$$\text{sim}(I_x, I_y) = |I_x \cap I_y| / 12$$

Figure 3b shows the code, $\phi(I_7)$, activated in response to I_7 . Black coding cells: cells that also won for I_1 , i.e., cells in $\{\phi(I_7) \cap \phi(I_1)\}$; red: winning cells not in $\{\phi(I_7) \cap \phi(I_1)\}$; green: non-winning (inactive) cells also in $\{\phi(I_7) \cap \phi(I_1)\}$. The intention of the red color for coding cells is that if this is a retrieval trial in which the model is being asked to return the closest matching stored input, I_1 , the red cells can be considered errors. Although, we note that the model as a whole would still be able to return the correct answer given that 18 out of 24 cells of I_1 's code, $\phi(I_1)$, are activated. However, if this was a learning trial, then the red cells would not be considered errors: this would simply be a new code, $\phi(I_7)$, being assigned to represent a novel input, I_7 .

Figure 3d shows the first key message of the figure, namely that the probabilities of the six stored hypotheses (i.e., the likelihood that the current input I_7 equals I_1 , that $I_7 = I_2$, etc.), are *simultaneously* active in proportion (with some statistical variance) to the pixel-wise similarity of I_7 with I_1 to I_6 , i.e., $L(I_x) \propto \text{sim}(I, I_x)$. The probability/likelihood scale is normalized to [0,1] by dividing code intersection size by the number of CMs, e.g.,

$$L(I_1) = |\phi(I_7) \cap \phi(I_1)| / Q$$

Thus, the blue bar in Figure 3d represents the fact that $\phi(I_7)$ has 18 out of 24 cells in common with $\phi(I_1)$: these are the black cells in Figure 3b. The cyan bar for I_2 indicates that $\phi(I_7)$ has 12 out of 24 cells in common with $\phi(I_2)$, where in general, many of these 12 may be common to the 18 cells in $\{\phi(I_7) \cap \phi(I_1)\}$. And so on for the other stored hypotheses. We note that even the code for I_6 which has zero intersection with I_7 has two cells in common with $\phi(I_1)$. In general, the expected code intersection for the zero input intersection condition is not zero, but chance, since in that case, the winners are chosen from the uniform distribution in each CM, thus: thus, the expected intersection in that case is just Q/K .

We acknowledge that the likelihoods in Figure 3d may seem high. After all, I_7 has less than half its pixels in common with I_1 , etc. Given these particular input patters, is it really reasonable to consider I_1 to have such high likelihood? Bear in mind that our example assumes that the only experience this model has of the world are single instances of the six inputs shown (as purely spatial inputs). We assume no prior knowledge of the underlying statistical structure generating the inputs. In this case, it is really only the *relative* values that matter and we could pick other parameters, notably in CSA Steps 6-8, that result in a much less expansive sigmoid, resulting in lower expected intersections of $\phi(I_7)$ with the learned codes, and thus lower probabilities. The main point is simply that the expected code intersections correlate with input similarity.

Figure 3c shows a second key message, which is that the likelihood-correlated pattern of activation levels of the codes (hypotheses) apparent in Figure 3d is achieved via independent soft max choices in each of the Q CMs. Figure 3c shows, for all 196 mac cells, the traces of the relevant variables used to determine $\phi(I_7)$. The raw input summation from active pixels is indicated by u . In this paper, all weights are effectively binary, though “1” is represented with 127 and “0” with 0. Hence, the maximum u value possible in any cell when I_7 is presented is $12 \times 127 = 1524$. The model in this example also assumes that all inputs will have exactly 12 active pixels (this can be relaxed but is assumed for simplicity). U is the normalized u value, as in Eq. 2, where $\pi_U = 12$. We assume $\lambda_U = 1$ here, thus by Eq. 3, $V_i = U_i$. A cell's V value represents the total *local evidence* that it should be activated. However, rather than simply picking the max V cell in each CM as winner (i.e., hard max), which would amount to executing only steps 1-4 of the CSA, the remaining CSA steps, 5-10, are executed, in which the V distributions are transformed as

described earlier and winners are chosen via soft max in each CM [final winner choices, chosen from the ρ distributions) are shown in row of triangles just under CM indexes]. Thus, a global function of the whole mac, G , is used to influence the local decision process in each CM. We repeat for emphasis that no part of the CSA explicitly operates on, i.e., iterates over, stored hypotheses; indeed, there are no explicit (localist) representations of stored hypotheses on which to operate.

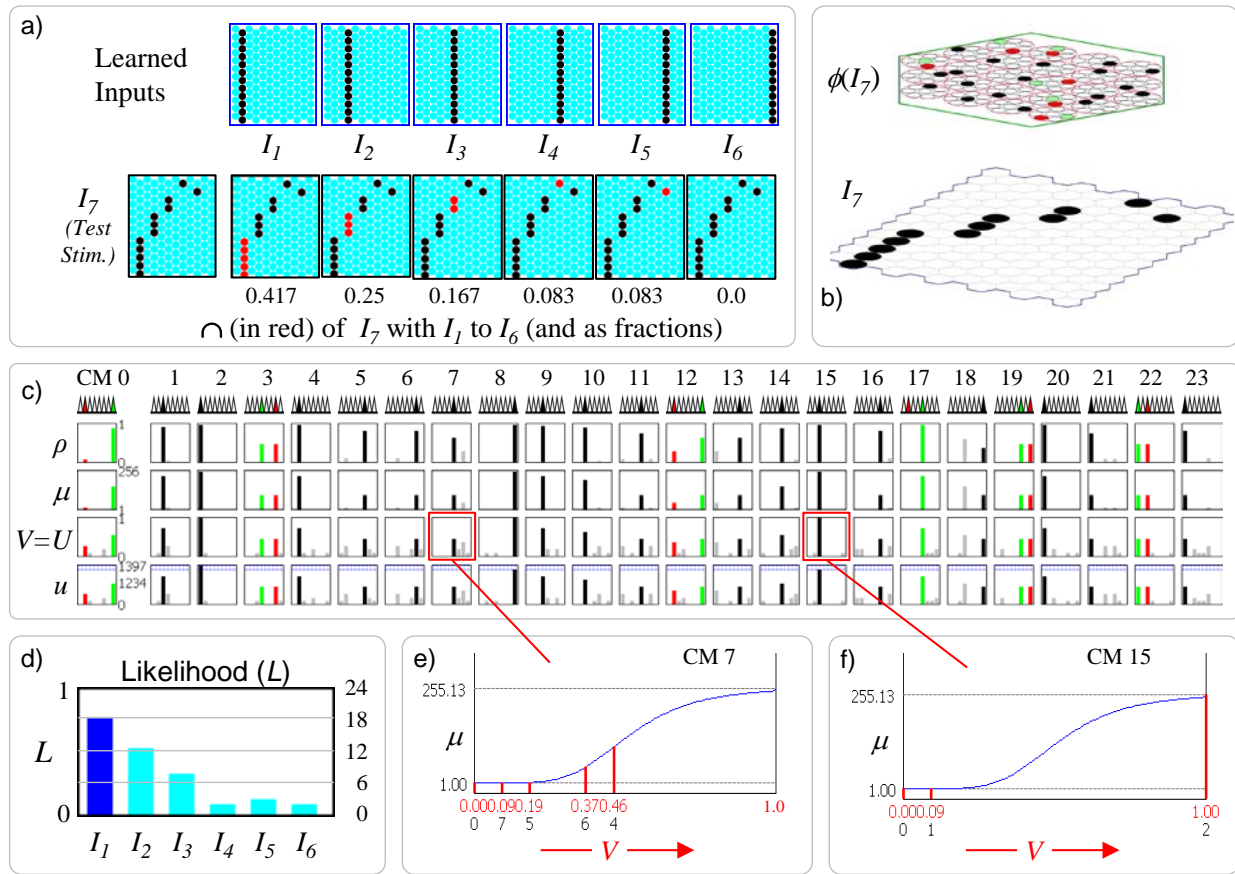


Figure 3: In response to an input, the codes for learned (stored) inputs, i.e., hypotheses, are activated with strength proportional to the similarity of the current input and the learned input. The test input I_7 is most similar to learned input I_1 , shown by the intersections (red cells) in panel a. Thus, the code with the largest fraction of active cells is $\phi(I_1)$ ($18/24=75\%$) (blue bar in panel d). The other codes are active in rough proportion to the similarities of I_7 and their associated inputs (cyan bars). (c) Raw (u) and normalized (U) input summations to all cells in all CMs. V values, which equal the U values in this purely spatial case, are transformed to un-normalized probabilities of winning (μ) in each CM via sigmoid transform whose properties, e.g., max value of 255.13, depend on G and other parameters. μ values are normalized to true probabilities (ρ) and one winner is chosen in each CM. Winners indicated in row of triangles: black: winner for I_7 that also won for I_1 ; red: winner for I_7 that did not win I_1 ; green: winner for I_1 that did not win for I_7 . (e, f) Details of V values for CMs, 7 and 15. Values in second row of V axis are indexes of cells having the V values above them. Some CMs have a single cell with much higher V and ultimately ρ value than the rest (e.g., CM 15), some others have two cells that are tied for the max (e.g., CM 3).

Figure 4 shows that different inputs yield different likelihood distributions that correlate approximately with similarity. Input I_8 (Figure 4a) has highest intersection with I_2 and a different pattern of intersections with the other learned inputs as well (refer to Figure 3a). Figure 4c shows that the codes of the stored inputs

become active in approximate proportion to their similarities with I_8 , i.e., their likelihoods are simultaneously physically represented by the fractions of their codes which are active. The G value in this case, 0.65, yields, via CSA steps 6-8, the V -to- μ transform shown in Figure 4b, which is applied in all CMs. Its range is [1,300] and given the particular V distributions shown in Figure 4d, the cell with the max V in each CM ends up being greatly favored over other lower- V cells. The red box shows the V distribution for CM 9. The second row of the abscissa in Figure 4b gives the within-CM indexes of the cells having the corresponding (red) values immediately above (shown for only three cells). Thus, cell 3 has $V=0.74$ which maps to approximately $\mu \approx 250$ whereas its closest competitors, cells 4 and 6 (gray bars in red box) have $V=0.19$ which maps to $\mu = 1$. Similar statistical conditions exist in most of the other CMs. However, in three of them, CMs 0, 10, and 14, there are two cells tied for max V . In two, CMs 10 and 14, the cell that is not contained in I_2 's code, $\phi(I_2)$, wins (red triangle and bars), and in CM 0, the cell that is in $\phi(I_2)$ does win (black triangle and bars). Overall, presentation of I_8 activates a code $\phi(I_8)$ that has 21 out of 24 cells in common with $\phi(I_2)$ manifesting the high likelihood estimate for I_2 .

To finish our demonstration for the spatial input case, Figure 4e shows presentation of another input, I_9 , having half its pixels in common with I_3 and the other half with I_6 . Figure 4g shows that the codes for I_3 and I_6 have both become approximately equally (with some statistical variance) active and are both more active than any of the other codes. Thus, the model is representing that these two hypotheses are the most likely and approximately equally likely. The exact bar heights fluctuate somewhat across trials, e.g., sometimes I_3 has higher likelihood than I_6 , but the general shape of the distribution is preserved. The remaining hypotheses' likelihoods also approximately correlate with their pixel-wise intersections with I_9 . The qualitative difference between presenting I_8 and I_9 is readily seen by comparing the V rows of Figure 4d and 4h and seeing that for the latter, a tied max V condition exists in almost all the CMs, reflecting the equal similarity of I_9 with I_3 and I_6 . In approximately half of these CMs the cell that wins intersects with $\phi(I_3)$ and in the other half, the winner intersects with $\phi(I_6)$. In Figure 4h, the three CMs in which there is a single black bar, CMs 1, 7, and 12, indicates that the codes, $\phi(I_3)$ and $\phi(I_6)$, intersect in these three CMs.

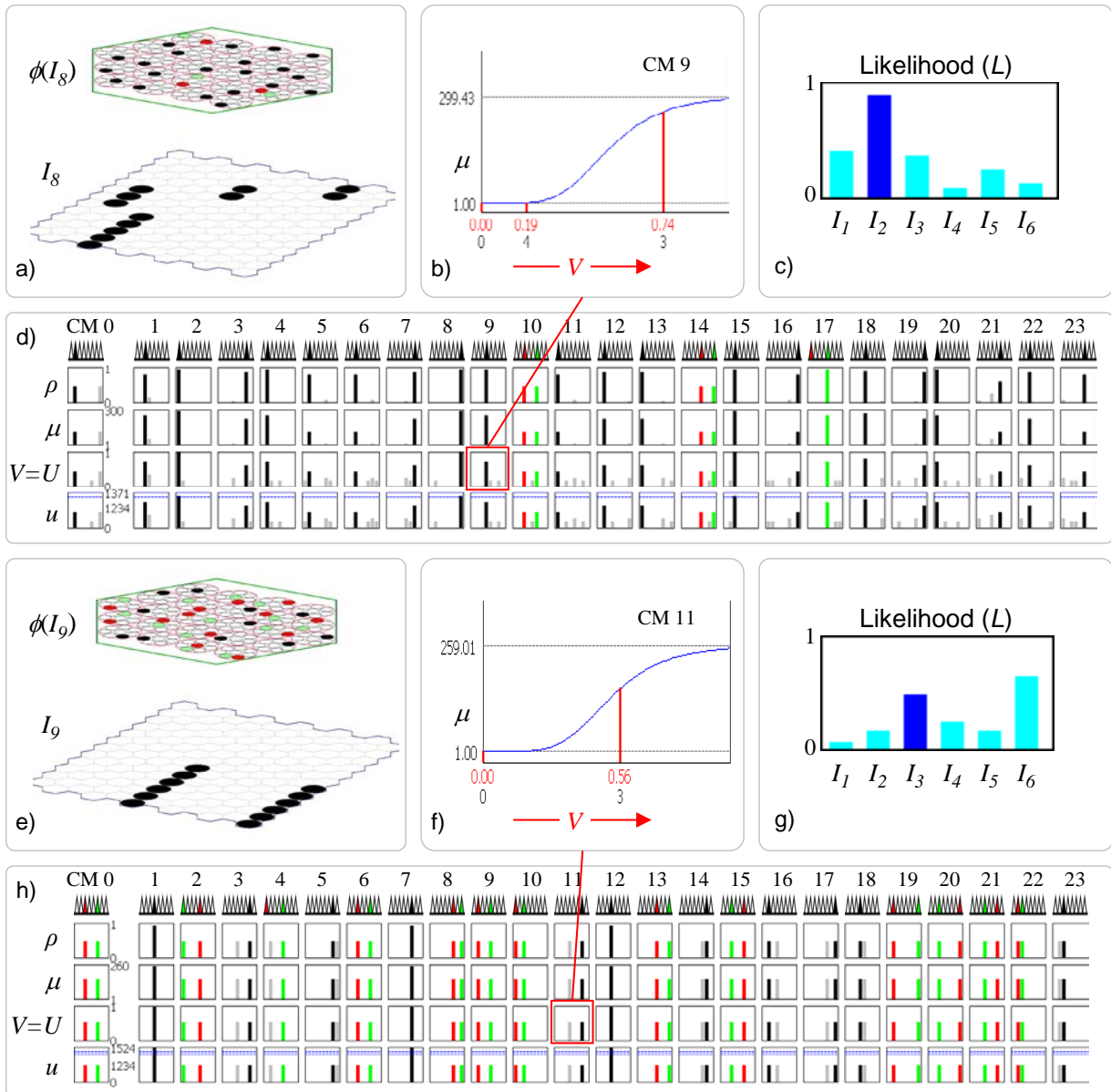


Figure 4: Details of presenting two further novel inputs, I_8 (panels a-d) and I_9 (panels e-h). In both cases, the resulting likelihood distributions correlate closely with the input overlap patterns. Panels b and f show details of one example CM (indicated by red boxes in panels d and h) for each input.

Single SDC Code Represents Entire Prob. Distribution: Spatiotemporal (Sequential) Case

In this section, we demonstrate the moment-to-moment (frame-by-frame) update of the similarity/likelihood distribution for the spatiotemporal, i.e., sequential, case. Figure 5 shows the training set consisting of two 4-item sequences, $S1=[ABCD]$ and $S2=[EFGH]$, where the items are the 12x12 pixel patterns shown. Figure 5 also shows two novel test sequences, $S3$ and $S4$, constructed from the same or slightly perturbed versions of the items comprising the training sequences. We will present the details of testing on $S3$ and $S4$, but begin by showing, as a baseline, the details of testing on a training sequence, $S1$, in Figures 6 and 7. The training sequences were handcrafted to show naturalistic edge motion patterns [given simple preprocessing (edge-filtering, skeletonization, and binarization) on a 12x12 aperture of the visual field] and such that the degree of pixel overlap amongst the frames is low. The test sequences were constructed so that their first and second halves would unambiguously be spatiotemporally most similar to the first and second halves of the training sequences. The overall goal of the demonstrations of $S3$ and $S4$ is to show that the likelihood distribution shifts to reflect, approximately, the spatiotemporal similarities of the stored hypotheses as we switch at mid-sequence between slightly noisy/perturbed versions of the two learned sequences.

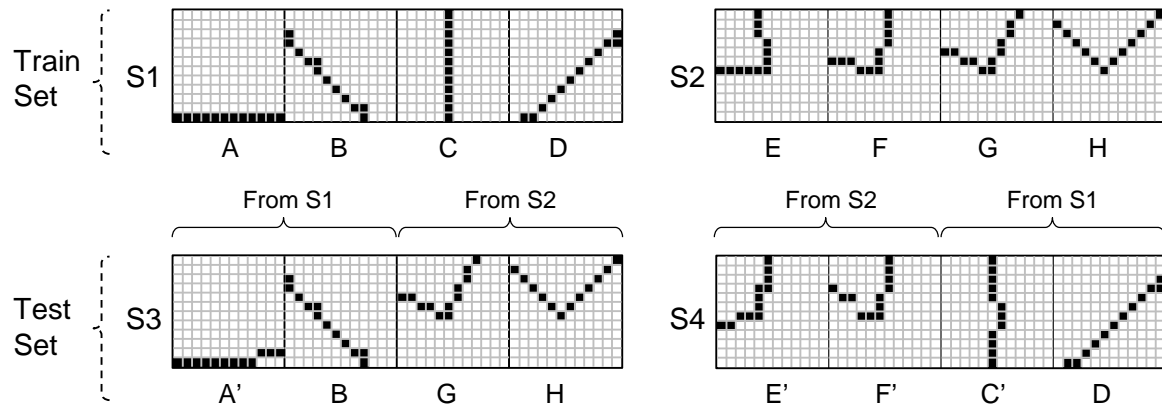


Figure 5: Train and test sequences used to demonstrate frame-by-frame update of the likelihood distribution for the case of spatiotemporal (sequential) patterns. The prime mark (‘) is used to indicate that the frame is a noisy/deformed version of the corresponding learning frame.

Figure 6 shows the state of the model, i.e., the input and the code activated in response, at the four moments of the test presentation of $S1$. A sample of the active afferent U (blue) and H (green) weights on each moment (frame) are shown. The cell at the source of an H weight will have been active on the prior moment. In panels, c and d, we show, for the selected cell, all U weights increased throughout learning: thus, it can be seen that the selected cell was active not just on the moment depicted [blue lines originating from active (black) pixels] but on other moments as well [blue lines originating from inactive (white) pixels]. This figure also introduces our *moment* notation. By ‘moment’, we mean a particular spatial input (sequence item) in the *context* of all the item sequence that preceded it from start of sequence, which we indicate by enclosing the sequence including the current item in brackets and bolding the current item.

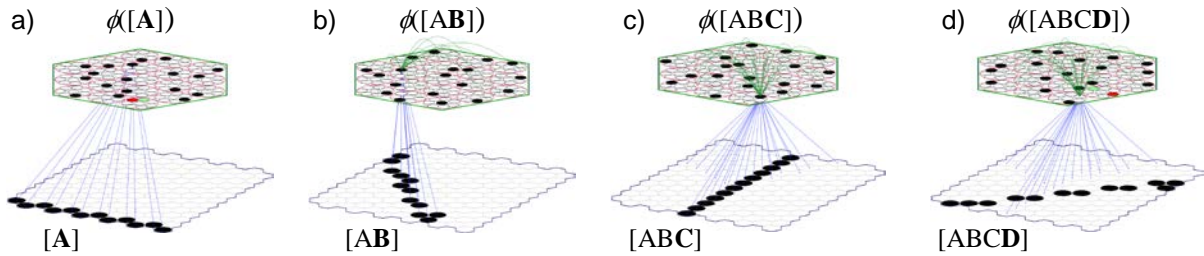


Figure 6: The state of the model at the four moments of the test presentation of S1.

Figure 7 shows the processing details when the training sequence S1 is presented as a test. Note that this model has $Q=19$ CMs each with $K=8$ cells. Also note that in this and subsequent figures, the U and V traces appear separately: they are identical for the first item but $V=HU$ for all non-initial sequence items. In total, eight spatiotemporal moments were stored in the mac during learning. S1's first moment is the presentation of its first item, A, denoted [A], followed by [AB], [ABC], and [ABCD], as shown in Figure 6. Similarly for S2's moments, [E], [EF], [EFG], [EFGH] (not shown).

The main message of Figure 7 is that the likelihoods of the eight stored hypotheses, i.e., the hypothesis that the current input moment is [A], that it is [AB], etc., are updated, with each successive item, in a way that, at least coarsely, respects the spatiotemporal similarity structure of the experienced inputs. A glance down across the four likelihood charts at right verifies this, showing that the code of the correct moment is activated almost perfectly on all four moments of S1, while the active fractions of the codes of other stored moments, i.e., their likelihoods, are much smaller. The one exception is in Figure 7c: while the actual input moment, [ABC] has the highest, and maximal, likelihood, moment [E] also has considerably higher likelihood than the others. This is appropriate and is due to the fact that item E has significant overlap with C (4 pixels), and when [E] was presented on S2's learning trial, the prior learning in the U weights that occurred when [ABC] was learned caused high u summations for the cells in $\phi([ABC])$ and consequently a relatively high intersection, $\{\phi([ABC]) \cap \phi([E])\}$.

Figure 7's charts show that the correct (at least coarsely) tracking of likelihood is achieved via *independent* soft max choices in each of the Q CMs. In panels b-d, in all CMs, the correct cell has $U=1$ and $H=1$, which yields $V=1$. This reflects that fact that the test sequence here is an exact duplicate of one that has been learned, S1. Many other cells have *either* a significant U or a significant H value, which is crosstalk and reflects the histories of other codes in which the cells were active, but not both. This yields zero or near-zero V values for all cells besides the correct ones, and thus, in every CM, a ρ distribution that greatly favors the correct cell. Two errors occur, one in CM 17 for moment [A] and one in CM 11 for moment [ABCD]: as winners are picked using *soft max*, there are occasional instances in which a far less likely neuron is selected. Nevertheless, we see that the effect of global familiarity, G , which equals one at all four moments, modulates the V -to- μ transform in such a way as to cause almost the whole stored code to activate, i.e., to increase the correlation of those cells. And, as will be seen in Figures 8 and 9, lower G values decrease correlation. Thus, our theory provides a causal, indeed normative, explanation of correlation in the brain. The degree of correlation from one moment to the next, both during learning and retrieval (inference), is effectively modulated (though indirectly) by a deterministic mechanism. That is, the modulation of the V -to- μ transform, indeed all CSA steps except for the last, are deterministic.

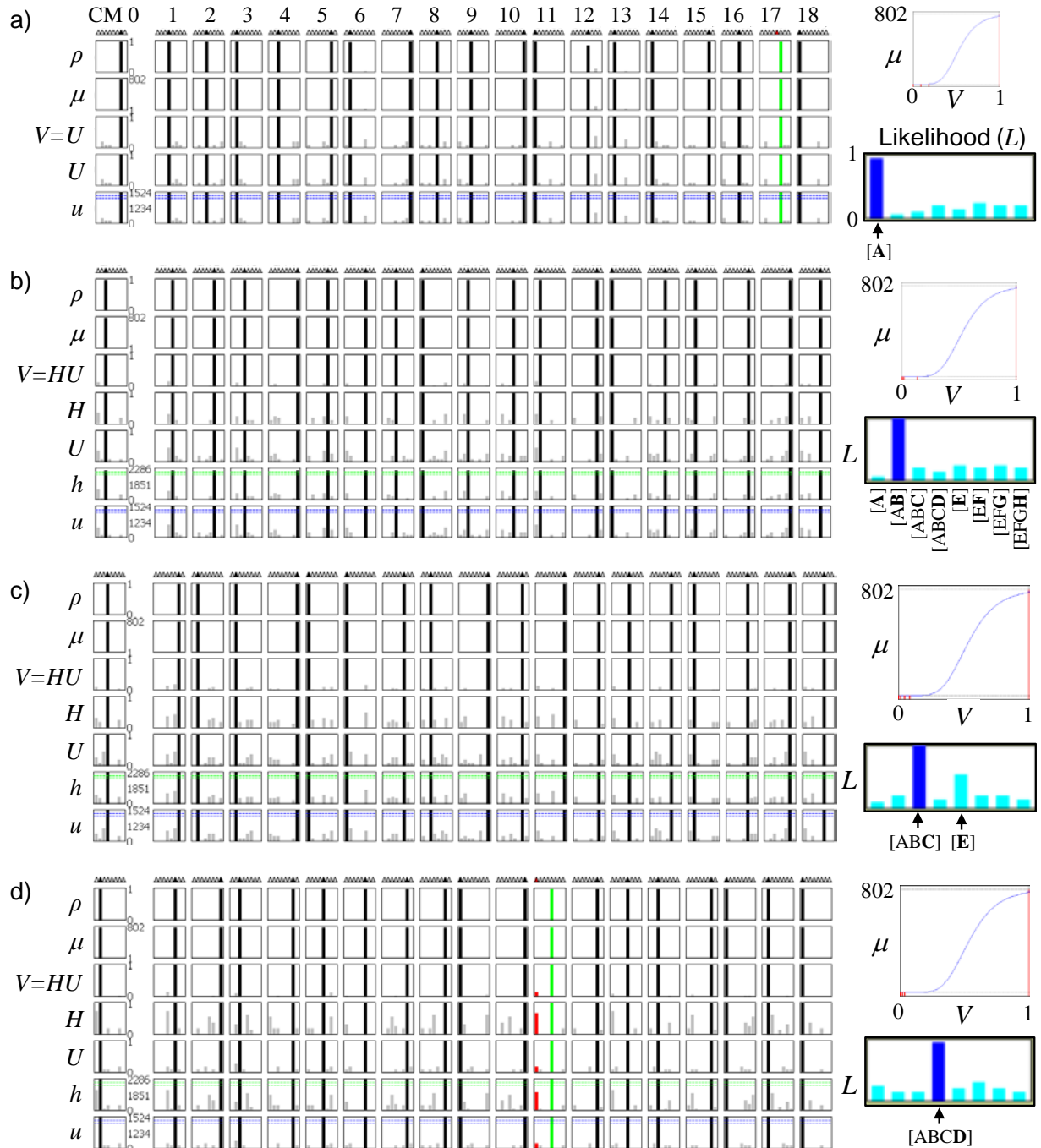


Figure 7: Detailed trace information for test presentation of all four items of S1=[ABCD]. Because S1 was also a training item and because only one other sequence has been stored in the mac (and thus, crosstalk is low), the model detects $G=1.0$ (100% familiarity) for each item and reinstates the traces almost perfectly. The V -to- μ function is the same at all four moments because $G=1$ in all four cases). The likelihoods over the eight moments stored in the mac are shown at right: the key for the eight moments is the same for all panels and is shown only in panel b to reduce clutter. Panel a has no h or H traces since they are not relevant on the first item of a sequence

We now consider two novel sequences as further evidence that hypothesis likelihoods, measured as active fractions of their SDC codes, approximately (coarsely) track the spatiotemporal similarity of the presented sequence from moment to moment. Figure 8 shows the state of the model at the four moments of both sequences, $S3=[A'BGH]$ and $S4=[E'F'C'D]$. As noted earlier, these sequences were constructed so that the relative spatiotemporal similarities of the stored (learned) moments and the current test moment would be clear even without an exact spatiotemporal similarity metric. That is, the first two moments of $S3$ must clearly be considered closest to the first two moments of $S1$. The third moment, $[A'BG]$ is *spatially* closest to the third moment of $S2$, $[EFG]$, but from a *spatiotemporal* perspective, i.e., considering the immediately prior two moments as context, the model should reasonably consider the learned moment, $[ABC]$ to also have elevated likelihood. The likelihood panel in Figure 9c indeed shows that the two moments, $[ABC]$ and $[EFG]$ have the two highest likelihoods. Their precise likelihoods vary across test instances, but they are almost always the two highest. This behavior is due to flattened distributions, resulting from the lower G ($=0.478$) and the fact that in many CMs, the cell that was in $\phi([ABC])$ and the cell that was in $\phi([EFG])$ are tied or nearly tied for the max V .

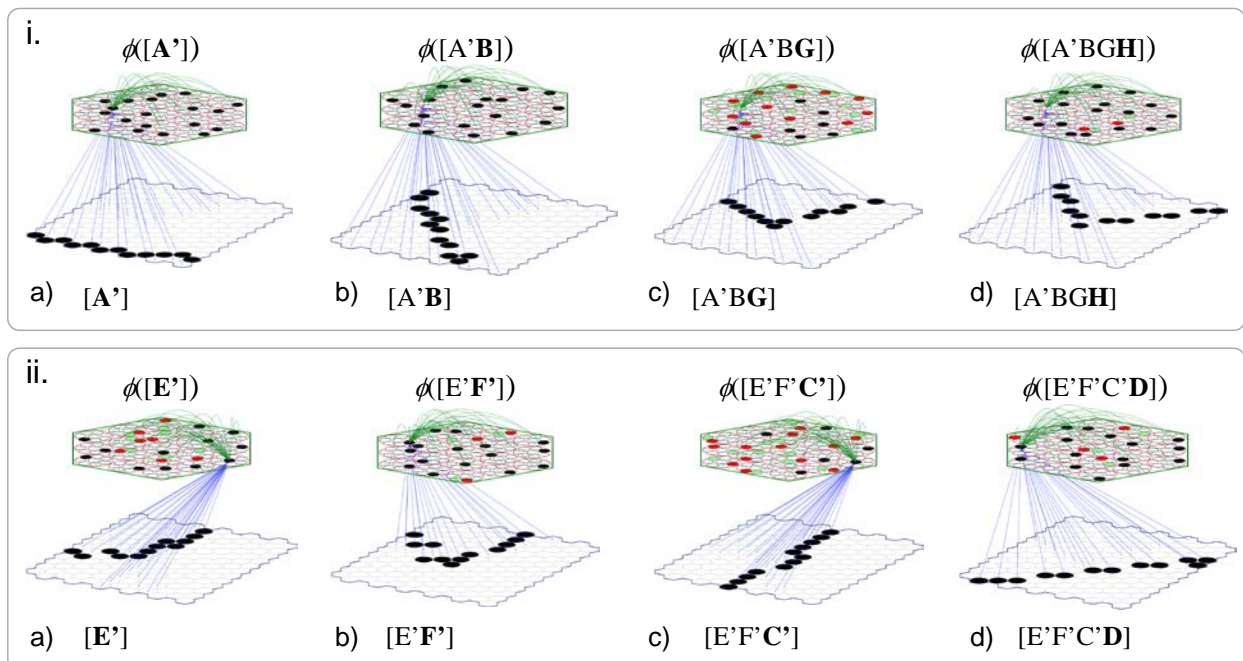


Figure 8: The state of the model at the four moments of each of the novel test sequences, $S3=[A'BGH]$ (i) and $S4=[E'F'C'D]$ (ii).

The same reasoning that allows us to consider $S3$'s third moment, $[A'BG]$ ambiguous, i.e., taking temporal context into account, suggests that the fourth moment, $[A'BGH]$, should be judged less ambiguous and in fact more likely to be an instance of learned moment, $[EFGH]$. This is indeed reflected in the likelihood panel in Figure 9d. The higher global familiarity, $G=0.566$, results in a more expansive V -to- μ transform, which, in combination with higher V values for the cells in $\phi([EFGH])$ results in those cells being greatly favored in each CM. Thus, the model is seen to have successfully gone through an ambiguous state of a sequence, recovering via the on-line combining of new evidence to yield an appropriately less ambiguous internal state.

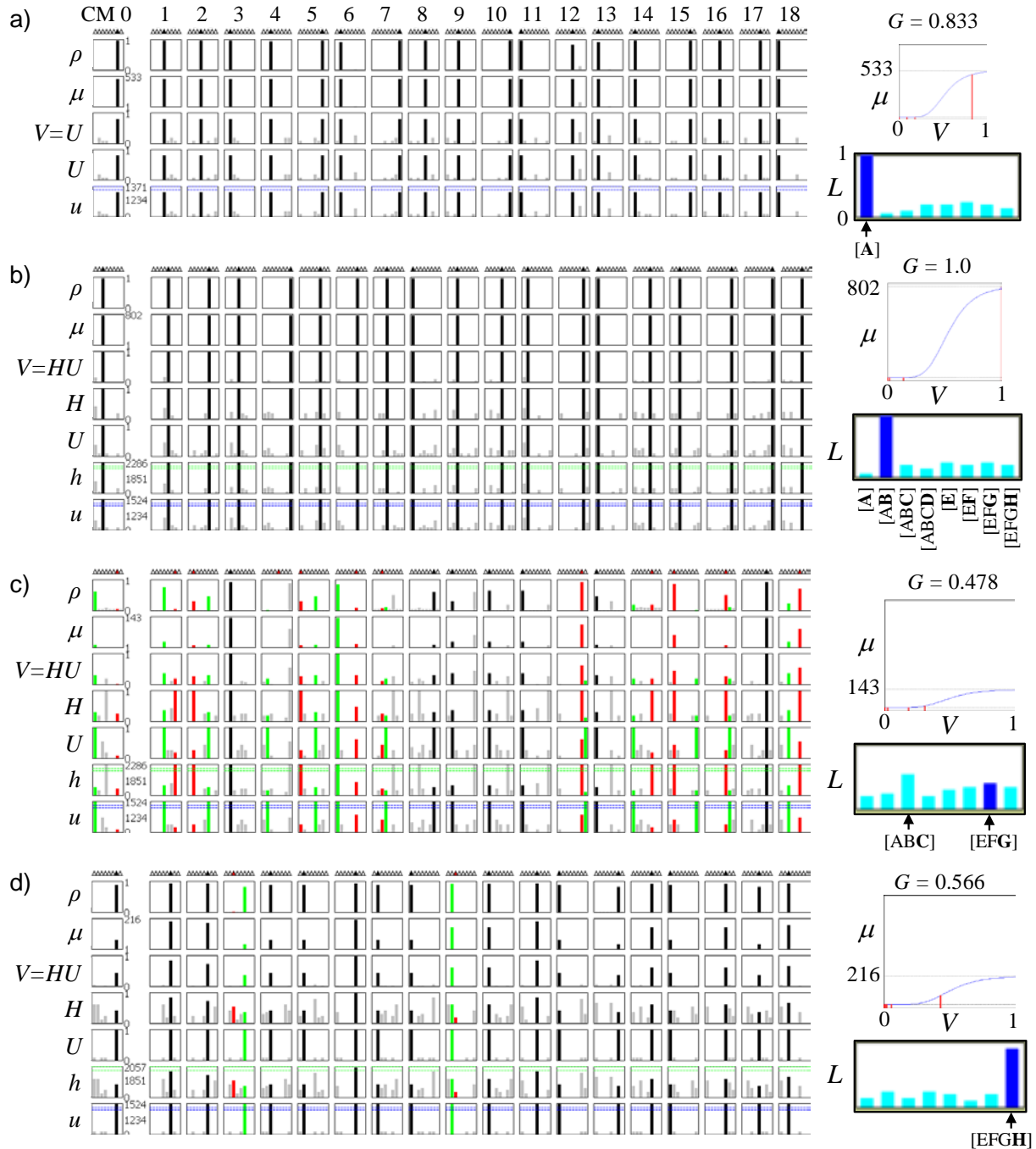


Figure 9: Detailed trace information for test presentation of all four items of $S3=[A'BGH]$.

Figure 10 shows the results for the final example, $S4=[E'F'C'D]$ whose first two moments were constructed to be closest to the first two moments of $S2$ and whose second two moments are very close to the last two moments of $S1$. The behavior of the model is broadly analogous to its behavior for $S3$ in that at its third moment, $[E'F'C']$, the two learned moments, $[ABC]$ and $[EFG]$, deemed most likely by the model are plausibly spatiotemporally most similar by the same reasoning applied for $S3$. Global familiarity, $G=0.314$, is lower here than for the third moment of $S3$ because we introduced more noise to the first two moments of $S4$ than to $S3$. In fact, the spatial input E' has the same intersection with E as it does with C (as can be seen in Figure 5) and F' has 9 of 12 pixels in common with F . Thus, learned moments, $[ABC]$

and [E], have approximately the same likelihood in Figure 10a. Although the cells comprising $\phi([ABC])$ were originally chosen in a spatiotemporal context and therefore had their afferent H weights increased [from the cells comprising $\phi([AB])$], there are no H signals present on the first item of any sequence. Thus, the choice of winners on the first moment of S4 depends only on U signals and thus, on the increases made to the U weights during learning. This is why learned moment [ABC] receives a high likelihood at this moment.

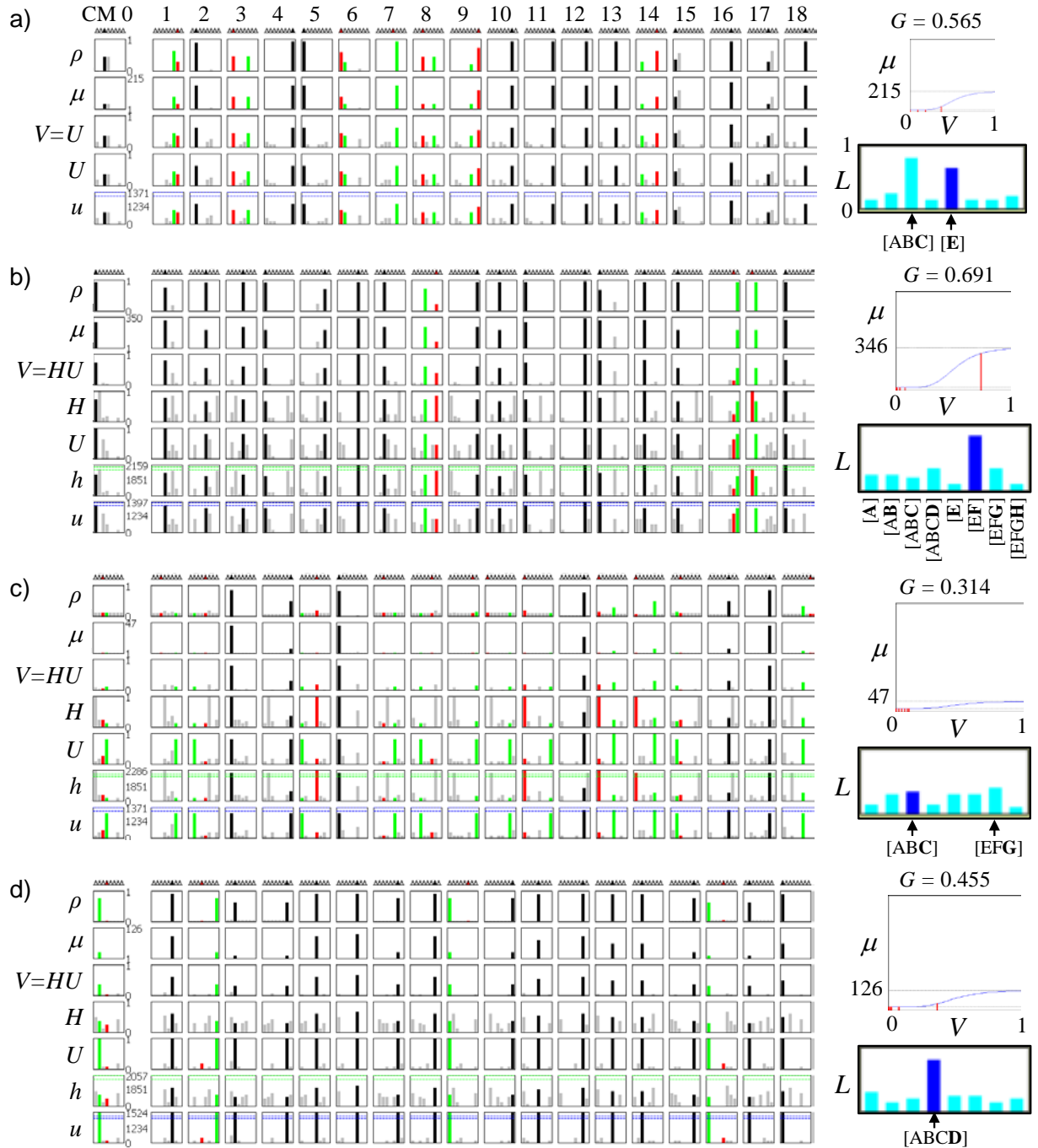


Figure 10: Detailed trace information for test presentation of all four items of S4=[E'F'C'D].

Figure 10b shows that the ambiguity present on the first moment is greatly diminished by the presentation of spatial input F' , which is quite similar to F , thus making the spatiotemporal moment, $[E'F']$ much more spatiotemporally similar to $[EF]$ than to $[ABCD]$ or to any other learned moment. On the third moment of S4 (Figure 10c), we present spatial input C' which is much more similar to C than any other of the spatial inputs. As was the case for the third moment of S3, this leads to the two learned third moments, $[ABC]$ and $[EFG]$ being approximately equally likely. However, due to the increased noise present in the first three moments of S4 compared to S3, G is lower here and the likelihoods of these two learned moments, i.e., the fractions of their codes active, are appropriately lower than was the case on the third moment of S3. Finally, we present spatial input D on the fourth moment, $[E'F'C'D]$. Due to the multiplication of the U signals from D and the H signals from $\phi([F'G'C'])$, which had appreciable overlap with $\phi([ABC])$, the cells comprising $\phi([ABCD])$ are highly favored in all CMs and end up winning in most of them, yielding the significantly higher likelihood for $[ABCD]$ than all other moments, as seen in Figure 10d.

Again, the model is seen to negotiate ambiguous moments, updating its active code from moment to moment, such that it simultaneously represents what are plausibly (given its small experience of the world) the most likely hypothesis (or hypotheses) and the full distribution over hypotheses. It has been pointed out that this ability, i.e., simultaneously representing multiple competing hypotheses, as for example is required for representing motion transparency, is problematic for theories which use fully distributed codes, as do the PPC theories (Pouget, Dayan et al. 2000). It is true that we do not go into numerical detail justifying most of the relative similarities/likelihoods (pair-wise and higher orders) present in the likelihood distributions of Figures 7, 9, and 10, nor, for that matter, those present in the spatial examples of Figures 3 and 4. However, our examples do demonstrate coarse correlation of spatial / spatiotemporal similarity with likelihood (measured as active fraction of code). Similar capabilities, such as being able to store and successfully recognize/retrieve large numbers of complex sequences, in which the same item(s) may occur multiple times and in varying contexts (e.g., a natural lexicon), have previously been demonstrated (Rinkus 1996, Rinkus 2014).

Classical Neural Tuning Functions as Artifacts

Neurons have classically been considered noisy because of high firing variability across presentations of the same stimuli. However, a great deal of the supposed noise/variability might actually be due to neurons having much more heterogeneous TFs than the Gaussian/Gabor TFs that have typically been assumed. Newer studies increasingly support this view (Cox and DiCarlo 2008, Rust and DiCarlo 2010, Mante, Sussillo et al. 2013, Nandy, Sharpee et al. 2013), especially for the spatiotemporal case (Nandy, Mitchell et al. 2016). Sparsey embraces this more modern view in that the TFs of individual cells, which emerge over the course of single/few-trial learning, are far less regular than the classical, unimodal, bell-shaped TFs. They are well described as being “multitaskers”, or having “mixed selectivity” (Fusi, Miller et al. 2016). Nevertheless, specifically because Sparsey does preserve similarity in the forward associative mappings, e.g., the U mapping from inputs to codes, it follows that similarity will also be preserved when considering that mapping in the reverse direction. That is, we expect to see lower-order statistical structure, e.g., the presence of one or multiple modes, in the reverse correlations for individual coding cells. In this section, we provide preliminary semi-quantitative support for the emergence of such TF structure, evidenced by reverse correlations, of single cells of Sparsey macs. This raises the possibility that the classical, unimodal, bell-shaped single-cell TFs that have been observed for 60+ years are simply artifacts of the underlying SDC-based learning/retrieval operations of the brain, or more pointedly, artifacts of using a) single/few-unit electrophysiology and b) low-complexity probe stimuli (e.g., bars, gratings), to observe the underlying SDC-based operations.

This study involved a multi-level version of Sparsey and thus, the full CSA, in (Rinkus 2014), which includes top-down (D) connections/signaling and other features. However, our focus here is only on the TFs of cells in macs at the first internal level (L1) and the fact that the more complex version of the CSA was used does not affect the conclusion. Figure 11a shows the 4-level Sparsey model instance with a 24x24-pixel input surface. This figure uses a rectangular pictorial format for the macs rather than the hexagonal format of the earlier figures. L1, proposed as analogous to a patch of cortical “V1”, is a 4x4 sheet of “V1” macs, each of which has a 6x6-pixel RF, or aperture. The semitransparent blue prism between aperture A_8^1 and mac M_8^1 is intended to suggest the completeness of the synaptic projection from A_8^1 's pixels to M_8^1 's cells. The input neurons (pixels) are binary and the apertures are disjoint (exactly tiling the input level). The disjointness is for simplicity: in general, Sparsey allows the RFs of macs at any level to overlap. Each V1 mac consists of $Q=9$ CMs, each having $K=16$ cells. The details of the higher level macs are unnecessary for this discussion. This model was exposed to 66 24x24-pixel binary edge-filtered 20-frame sequences processed from the KTH natural video data set (Schuldt, Laptev et al. 2004). Figure 11b shows the leading eight frames of eight of these sequences, which were presented once each during training.

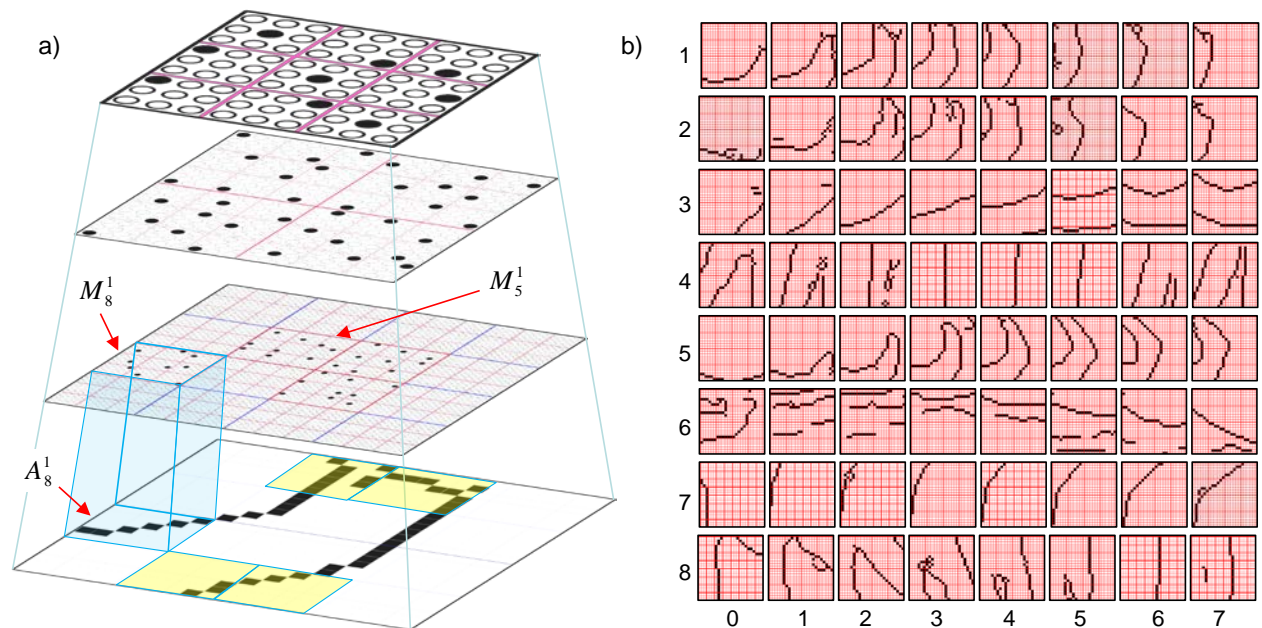


Figure 11: a) 4-level Sparsey model with 4x4 sheet of “V1” macs, each with a 6x6-pixel receptive field. b) Sample of the sequences presented to the model during training. (Note: the bolder red hatching in some frames is an artifact.)

Across the presentation of all 1,320 frames of the training set, every time an L1 mac became active the U wts from those active pixels to the $Q=9$ cells comprising the active code were increased to the max synaptic weight, 127 (binary “1”), unless already increased in which case it was left unchanged. Also note that in this study, in order for a V1 mac to activate, it had to have between 5 and 7 active pixels (out of 36) active in its RF. Thus, a given V1 mac might activate 10’s to 100’s of times over the course of the training. Most of those activations will be in response to unique inputs, which would typically beget unique SDC codes. Any particular one of a mac’s $QK=144$ cells will generally become active in many of those codes. For any such cell, we can compute the average of the input patterns in whose codes that cell was included, i.e., to which that cell responded, i.e., reverse correlation, giving us an *indirect* view of that individual cell’s TF, i.e., surrogate TFs. It’s an indirect view because the pixel gray levels do not represent the afferent

weights to the cells themselves (which are binary), but rather the frequencies of occurrence of the given binary pixel when the cell is active.

Figure 12 shows a sample of such TF surrogates for 40 cells selected from various of the 16 V1 macs. The number of codes in which a cell participated is given under its TF. The primary result visible in Figure 12 is that these single-unit surrogate TFs have a great deal of higher-order structure and in some cases, have some resemblance to classical V1 cell TFs. We underscore this resemblance by overlaying several TFs from one of Hubel & Wiesel’s seminal papers (Hubel and Wiesel 1962), directly on top of our model’s single-cell surrogate TFs. Furthermore, some of them evince multi-selectivity (Fusi, Miller et al. 2016). For example, the top left cell looks like it has been part of codes activated in response to vertical edges along the left side of the field and to diagonal (135°) edges. Similarly, the fifth cell in the second row looks like it has been part of codes for vertical edges occurring in the left and right halves of the field.

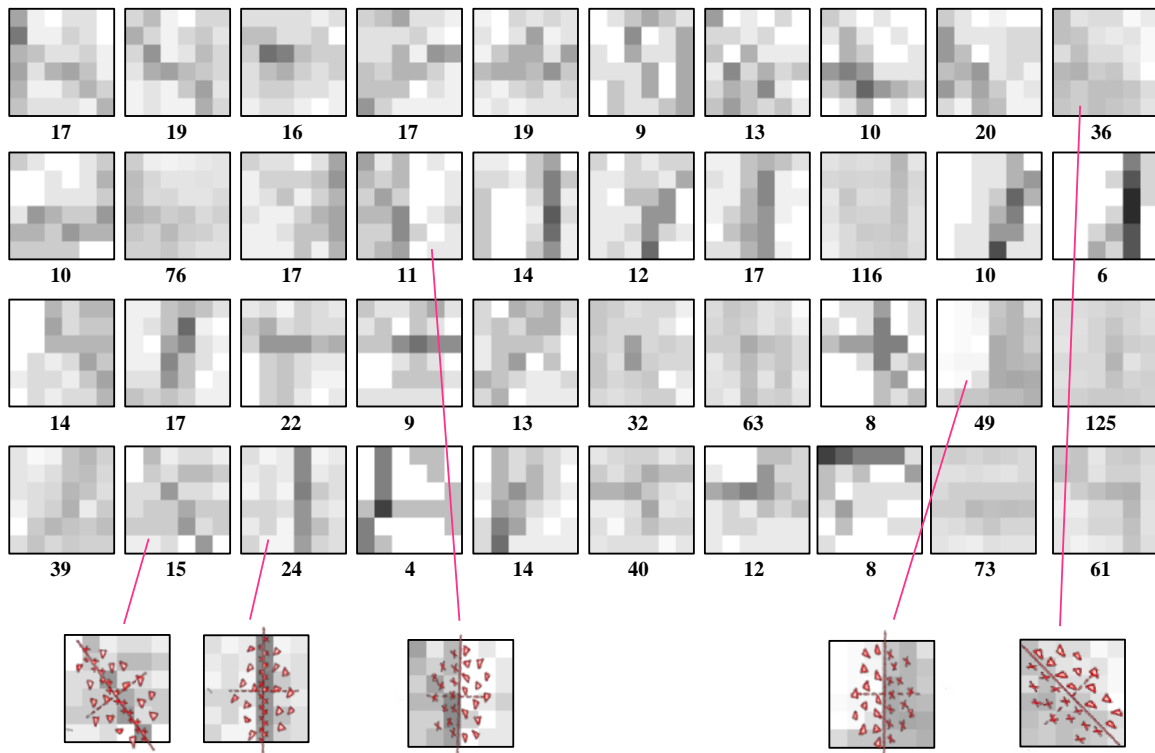


Figure 12: Reverse correlations showing indirect depictions of the tuning functions (TFs) of several of the model’s V1 cells (from various of the 16 V1 macs) showing a resemblance to classically observed single-cell TFs. At bottom, we overlay TFs from Hubel & Wiesel (red) on some of our model cell surrogate TFs to emphasize the resemblance. The number of SDC codes in which a cell participated [and thus, over which the “reverse correlation” (averaging, normalizing and representing in grayscale) is performed] is shown below each surrogate TF.

The surrogate TFs in Figure 12 are semi-quantitative as we have not computed their statistical significance, and so must be considered preliminary. However, the deviation from the more homogeneously gray fields that would be produced by chance, especially for higher cell usage counts, e.g., 20-50, indicates that cell win probability (within its CM) is being influenced by pairwise and higher-order pixel co-occurrences, or in other words, that cells are acquiring sensitivity to *features*, or to multiple features, in the input space. Again, we emphasize that all cells’ TFs are perfectly flat initially and that the surrogate TFs in Figure 12 emerge during learning via incremental superposition of *en masse* Hebbian updates to whole

SDC codes based on single trials. This suggests a novel explanation for the formation of the classical single-cell TFs, that have been observed in cortex for 60+ years.

It should be understood that if we let this system train indefinitely, then for most if not all L1 macs, all U weights to all their cells would eventually be increased to binary “1”. In that case (fully saturated U matrix), in each CM, all K cells would have equal and maximal u summations, which would ultimately activate a random code given any input, i.e., complete information loss. To avoid this, the full Sparsey model (Rinkus 2014) uses a critical period mechanism which stops further learning after a certain fraction of the U weights (to any given mac) have been increased. However, for this section’s example, the total number of inputs presented during learning is small enough that weight saturation is not an issue. That is, for most of the 2,304 ($9 \times 16 \times 16$) L1 cells, most of their afferent U weights are still zero after training.

Comparison of Recurrent SDC and Localist Representations of Latent Variables

In this conceptual section, we further underscore Sparsey’s novelty, in this case by clarifying the difference between a recurrent SDC concept of representing/computing with probabilities and that present in graphical probability models (GPMs), which have been cast almost exclusively in localist terms, i.e., individual latent variables and even individual values of variables are identified with single representational units. Figure 13 makes the difference clear. It underscores that not only are the *states* of the latent variables themselves represented differently in localism vs. SDC, but so are the *relationships* amongst the states (or more generally amongst the latent variables themselves). Figure 13 (bottom center) shows a hypothetical hidden Markov model (HMM) state transition graph. In Sparsey, the individual states would be represented by unique (though possibly overlapping) SDC codes (shown around perimeter, color-keyed). At top center, we show that relationships, e.g., $p(S2|S1)$, are represented *collectively* by *ensembles* (in fact, *sparse distributed subsets*) of synapses [cf. *synapsembles* (Buzsáki 2010)] rather than by single (*localist*) values as is the case for the traditional HMM. We reiterate that our SDC-based concept requires only binary synapses and units. Here, for example, the instantaneous value of $p(S2|S1)$ is measured by the fraction of S1’s code that is active. As we stated in the Introduction (point “A”), communicating this conditional probability (recurrently to the computations on the next temporal moment) is accomplished by the cells simply summing their (binary) H inputs. (These will then be combined with bottom-up (U) signals on the next moment as per the CSA to choose a next active SDC code and thus, the next active complete probability distribution.)

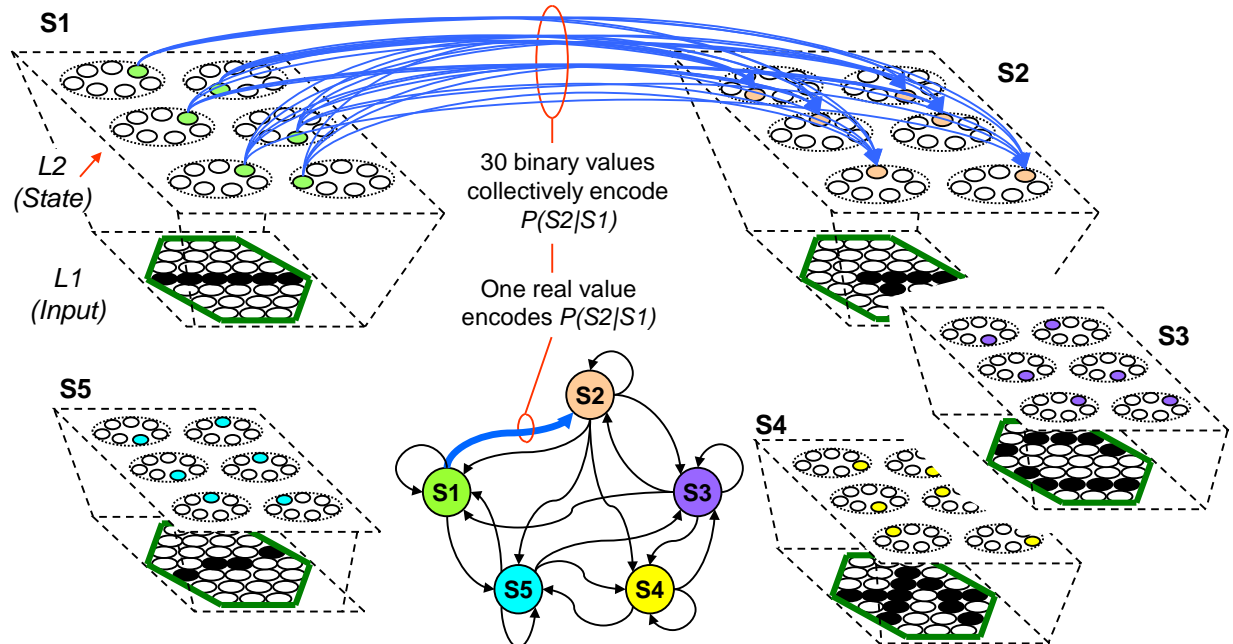


Figure 13: Relationship of Sparsey's representation of latent variables (and their specific values) and their relationships to their representation in a traditional, i.e., localist, graphical probability model, in particular, a Hidden Markov model (HMM). In the Sparsey version, there is a single recurrent SDC field (L2) comprised of $Q=6$ CMs, each with $K=7$ units, and we assume full recurrent (i.e., horizontal, H) connectivity of L2. Each state is represented by a unique SDC code (around perimeter, color-keyed to corresponding localist representations in the HMM state model at center). The relationship of S1 and S2, $p(S2|S1)$, is *collectively* quantified by a bundle of 30 binary H synapses, as opposed to a single, localist, real value as in the localist case. The instantaneous value of $p(S2|S1)$ is measured by the fraction of S1's code that is active.

We will not delve into the many additional issues/questions raised by this figure, except for the following key points.

1. The number of unique codes possible in this example is $Q^K=7^6$. While, in practice, only a small fraction can be assigned while maintaining functionality (due to accumulating crosstalk as additional codes are laid down in superposition), empirical (Rinkus 1996) and theoretical (Gripon, Heusel et al. 2015) evidence suggests the number of codes storable is certainly much larger than the number of units, which is the localist limit.
2. New latent variables can emerge (be learned, on-line) as new SDC codes, or as new clusters of codes (in the Q -dimensional code space), without requiring additional allocation of units/weights. As noted in the discussion, this is an important similarity between our work and that of (Pitkow and angelaki 2016, Rajkumar and Pitkow 2016). which stand in distinction to *infinite state* GPMs, e.g., (Doshi-Velez, Wingate et al. 2011), which address the need for GPMs to be able to discover a domain's latent variables, and their valuedness, and their conditional independence relations on-the-fly, but which are localist. Moreover, there is no essential distinction between different latent variables and different values of variables in the SDC formulation: they are just SDC codes (or sets of codes, or patterns of intersections over sets of codes).
3. Representing (conditional probability) relationships as synapsembles, rather than single real/graded-valued synapses, allows for much greater flexibility and speed of learning (as well as robustness to damage). The synapses of a given synapsemble are *bound* together in a unitary

event, e.g., experiencing an instance of S2 following S1, by virtue of all being increased similarly. However, each synapse will generally be involved in representing numerous relationships, i.e., be part of numerous synapsembles, and those synapsembles will generally overlap just as SDC codes themselves do. Future learning will generally modify the pattern of intersections (of all orders) of synapsembles, ultimately resulting in subsets of synapsembles (and corresponding subsets of coding units) which represent a domain's major statistical/structural regularities, i.e., its latent variables.

As we said, this section is a conceptual sketch and developing more quantitative analyses and demonstrations of these concepts is one of future research goals.

Discussion

We described a radically different theory, from the prevailing probabilistic population coding (PPC) theories, for how the brain represents and computes with probabilities. This theory avails itself only in the context of *sparse distributed coding* (SDC), as opposed to the fully distributed coding context in which the PPC models have been developed. The theory, Sparsey, was introduced 20 years ago [originally called TEMECOR (Temporal Episodic Memory using Combinatorial Representations)], as a model of the canonical cortical circuit and a computationally efficient explanation of episodic and semantic memory for sequences, but its interpretation as a way of representing and computing with probabilities was not emphasized. The PPC models (Georgopoulos, Kalaska et al. 1982, Zemel, Dayan et al. 1998, Pouget, Dayan et al. 2003, Sanger 2003, Jazayeri and Movshon 2006, Ma, Beck et al. 2006, Rajkumar and Pitkow 2016) share several fundamental properties: 1) continuous (graded) neurons; 2) *all* neurons formally participate in every code; 3) due to 1 and 2, synapses must either be graded or rate-coding must be used to allow decoding; 4) generally assume rate-coded signaling; 5) individual neurons are generally assumed to have unimodal, e.g., bell-shaped, tuning functions (TFs); 6) individual neurons are assumed to be noisy, e.g., firing with Poisson variability; and 7) this noise and correlation, e.g., noise correlation, is generally viewed as degrading computation and needs to be mitigated, e.g., averaged out.

In contrast to these PPC properties/assumptions, Sparsey assumes: 1) binary neurons; 2) individual codes are small (relative to whole coding field) sets of cells (SDCs) and any such code *simultaneously* represents both the best matching stored hypothesis and the similarity distribution over *all* stored hypotheses; 3) only binary synapses; 4) signaling via waves of contemporaneously arriving first-spikes from afferent SDC codes; 5) all afferent weights to coding neurons are initially zero, i.e., the TFs are initially completely flat, and emerge via single/few-trial learning to reflect a cell's specific history of inclusion in codes; 6) neurons are not assumed to be intrinsically noisy and are simply on or off on any given computational cycle (we do not require a spiking model); and 7) noise is a resource that is explicitly generated and injected into the code selection process to achieve a specific coding goal, namely that the overall set of codes stored in a coding field has the SISC property, which manifests, indirectly, as a particular correlation pattern. Thus, Sparsey entails a completely different view of noise/correlation from the mainstream. Rather than being viewed as a problem imposed by externalities (e.g., common input, intrinsically noisy cell firing), it essentially functions in a positive sense, i.e., as a resource.

Specifically, we showed that: a) if a model uses SDC coding; b) if the model's process of assigning SDC codes preserves similarity from the input space into the code space (the SISC property); and c) if input similarity correlates with likelihood, then the active SDC code simultaneously represents both the most probable hypothesis and the probability distribution over all stored hypotheses. Specifically, the probability of any hypothesis is represented by the fraction of its code's cells that is active in the single fully active code. We showed that in the spatiotemporal (sequential) case, with each successive sequence item,

Sparsey's core algorithm, the *code selection algorithm* (CSA) (Table 1), updates the entire distribution [cf. belief update (Pearl 1988)] in approximate accord with intuitive notions of spatiotemporal similarity.

Crucially, as can readily be seen in the CSA, Sparsey performs this update in *fixed time*, i.e., time that remains constant over the life of the system even as the number of stored hypotheses (memories) grows. We noted that this computational efficiency for both learning and retrieval has not been claimed for any hashing method, either neurally-relevant (Salakhutdinov and Hinton 2007, Salakhutdinov and Hinton 2009, Grauman and Fergus 2013), or more generally [reviewed in (Wang, Liu et al. 2016)]. Although time complexity considerations like these have generally not been discussed in the PPC literature, they are essential for evaluating the overall plausibility of models of biological cognition, for while it is uncontentious that the brain computes probabilistically, we also need to explain the extreme speed with which these computations, which are over potentially quite large hypothesis spaces, occur.

The key to Sparsey's computational speed is its extremely efficient method of computing the *global* familiarity, G , of an input (to a mac), and using G to adjust an individual cell's transfer function from its own local similarity measure, V , to its final probability, ρ , of being chosen winner [in its own winner-take-all competitive module (CM)]. G can be viewed as directly modulating the noise present in the process of code selection. That is, when high familiarity is detected, noise is minimized by disproportionately increasing the bias towards selecting cells that are more correlated with input (higher correlation being indicated by higher V), i.e., *pattern completion*, and when low familiarity is detected, noise is maximized by making win probability of all cells in each CM more equal (when $G=0$, all cells are equiprobable), i.e., *pattern separation*. See (Rinkus 2010) for a sketch of a possible noise modulation mechanisms involving one or more of the brain's neuromodulators. We emphasize that this mechanism constitutes a radically novel concept of noise and correlation in the brain. Moreover, it constitutes a novel method for combining global and local information during inference (and learning). In particular, it suggests the possible necessity of a structural *mesoscale* (in our case, the WTA CM) to facilitate the use (mixing) of global information into the local decision processes.

In addition to Sparsey's efficiency from a purely algorithmic standpoint, we emphasize that because it requires only binary neurons and synapses, it does not require rate coding. Rather, it is naturally suited to signaling via waves of contemporaneously arriving first-spikes from one SDC code to the next, either recurrently or to downstream coding fields. Thus, rather than the ~100 ms that reliably decoding spike frequency requires, our model requires only a few ms window during which contemporaneous signals from an afferent SDC code might arrive at a downstream coding field and be integrated. We imagine that some sort of macrocircuit-level control apparatus, e.g., integration during some phase of a gamma-scale envelope [cf. (Buzsáki 2010)], might impose such a window, a hypothesis we would like to explore in the future. We also emphasize the potentially significantly lower metabolic/energy costs of signaling based on first-spikes compared to signaling via rate-coding (in which many spikes must be sent and integrated). This is in addition to the already reduced energy costs of sparse coding compared to dense coding.

Sparsey is an existence proof that representing and using graded values, e.g., probabilities, requires only binary neurons and binary synapses. As elaborated upon in the last Results section, there is no need for explicit *localist* representation of graded values, anywhere in the system/computation. More specifically, there is no need to represent probabilities/likelihoods as spatially localized firing rates (i.e., at particular synapses) and there is no need to represent conditional probabilities, or strengths of association, via continuous/graded weights.

In addition to being a radically new explanation for how the brain represents and computes with probabilities, we presented a perhaps even more provocative result giving preliminary evidence that the

classical, unimodal, bell-shaped TF, ubiquitously observed for over 60+ years of experimental neuroscience and which constitutes a fundamental building block of the theoretical edifice, is simply an *artifact* of: a) what the brain is actually doing, i.e., laying down SDC codes in superposition based on single trials; and b) the limitations of experimental methods, i.e., single/few-unit electrophysiology and low-complexity probe stimuli. Our results show that in the framework of sparse distributed coding, single/few-trial Hebbian learning operating on binary neurons and synapses can yield what look very much like classical one/few-mode TFs. Consistent with other recent opinions (Yuste 2015, Fusi, Miller et al. 2016, Schneidman 2016), Sparsey evinces a move beyond the ‘Neuron Doctrine’ to a new paradigm in which the ensemble (SDC, cell assembly), not the single neuron, is the fundamental functional unit of neural computation, i.e., of thought (cognition).

As Sparsey is a distributed memory, the traces are stored in superposition and therefore interference (crosstalk) does increase with the number of hypotheses stored. For a given setting of parameters, there will be regime in which the number of stored hypotheses is low enough so that expected interference, i.e., expected retrieval error, remains tolerable. If the overall Sparsey system had only one internal level and only one mac at that level, then analyses characterizing capacity, expected errors, vis-à-vis parameters, would be the primary research focus. But, this is not the case. The single Sparsey module, the mac, is proposed as the analog of the cortical macrocolumn. And, the cortex is known to be organized as a deep hierarchy, with perhaps >10 cortical level (along some paths), where each level is a patch of order hundreds to thousands of macs. The question of overall storage capacity as it relates to explaining the apparent vast storage capacity of the typical human over most of his lifespan will thus depend on how information is distributed throughout the entire hierarchy, not just in a single mac.

The advantages of organizing knowledge hierarchically, both categorically and componentially (part-whole) have long been known. More recently, the advantages of many-leveled vs. flat representations have been described in terms of the efficiency (essentially, the number of parameters needed) of representing highly nonlinear relations (Bengio 2007, Bengio, Courville et al. 2012) and the constant stream of impressive “Deep Learning” results strongly bears this out (Krizhevsky and Hinton 2011, LeCun, Bengio et al. 2015, Silver, Huang et al. 2016). However, Deep Learning models, including LSTM (Hochreiter and Schmidhuber 1997), have thus far not been combined with SDC, and indeed, the principles of the two paradigms are very different and may be essentially incompatible. In this regard, we must specifically point out that the recently described Sparsely-Gated Mixtures of Experts model (Shazeer, Mirhoseini et al. 2017), while exploiting a principle of sparsity (referred to more generally as *conditional computation* in which the explicit goal is to minimize the fraction of the machines parameters participating in any given computation), is not an instance of SDC as present in Sparsey and other SDC models and has numerous differences from SDC-type models, notably, that it has been developed in a supervised context and uses Backpropagation.

We have also been exploring multi-level hierarchies, but of SDC coding fields, e.g., the model used in our explanation of single-cell TFs, and will be continuing on this path. We believe that truly capturing the essence of how the brain computes requires the union of hierarchy/heterarchical organization and *sparse* distributed coding, which places our work in distinction with, on the one hand, Deep Learning models, which combine *densely/fully* distributed coding fields (i.e., Boltzmann or MLP fields) with hierarchy [though (Shazeer, Mirhoseini et al. 2017) appears to be an exception], and on the other hand, HMAX models (Riesenhuber and Poggio 1999, Riesenhuber and Poggio 2002, Serre, kouh et al. 2005, Poggio and Serre 2013), which combine *localist* coding fields with hierarchy.

However, there is another, new theory of probabilistic computation in the brain, for which distributed representation is essential, and which is much closer in spirit to Sparsey (Rajkumar and Pitkow 2016). Despite the fact that their theory shares most of the PPC properties mentioned at the outset, at a high level,

Sparsey can be described in terms quite similar to those used by (Pitkow and Angelaki 2016), which describes their theory as having three main parts: a) overlapping patterns of population activity are proposed to encode the latent variables of the observed domain; b) the brain specifies how those variables are related to the world through a sparse probabilistic graphical model; and c) recurrent circuitry implements a nonlinear message-passing algorithm that effectively executes probabilistic inference amongst the latent variables represented in the population codes residing in a hierarchy of coding fields. The analog of point (a) in a Sparsey mac is that the ‘overlapping patterns of population activity’ correspond to subsets of cells, i.e., intersections, that occur in multiple codes, i.e., across multiple contexts. These subsets are of size smaller than the whole code size, Q , and crucially, they emerge over the course of learning. Furthermore, there will in general be intersections over these subsets as well, allowing for the encoding of statistics of a range of higher orders. The analog of point (b) is that the modifications made to Sparsey’s synaptic projections, including the recurrent projection of a mac to itself and its U, H, and D, projections to/from other macs at its own and other levels of the hierarchy embed the conditional probabilistic relations amongst the latent variables. Sparsey’s analog of point (c) is essentially the operation of the CSA. These characteristics mean that these models can be viewed as distributed instantiations of graphical probability models (GPMs), which by large, have been localist, e.g., hidden Markov models, Bayesian nets, dynamic Bayesian nets. As discussed in the last section of Results, the move from a localist GPM concept to a distributed GPM concept has major implications, notably: i) that the domain’s latent variables (their identities and valuedness) are mapped to distributed codes which emerge over the course of on-line learning; and ii) that the conditional probabilistic relations amongst the variables are represented partially in the code intersections and partially in intersections of synaptic mappings (i.e., synapse-ensemble intersections).

After many decades, experimental methods are finally reaching the point where the fast time scale activities of all neurons in large, e.g., macrocolumn-scale, volumes will be observable. This will finally allow us to understand the brain’s operation in what we believe is its native language, essentially cell assemblies and sequences of cell assemblies (Hebb 1949), where in our view, each such assembly functions both as the most likely hypothesis (stored memory) and the distribution over all memories stored (in the cell assembly’s container, which we propose is the cortical macrocolumn). We offer Sparsey as theoretical elaboration of this concept, one which is simple, i.e., binary cells and synapses, single-trial Hebbian learning (with some additions, e.g., decay, in the fully general model), and general, in that the CSA is extremely generic, and powerful, in terms of its computational efficiency. There are numerous questions to pursue, notably regarding the nature/capacities of hierarchical interactions amongst macs and through time and we look forward to continuing to explore them.

Methods

Similarity Metric

The similarity metric for the case of spatial inputs is simply pixel-wise overlap. If all inputs have exactly the same number of active pixels, we can measure spatial similarity simply as size of intersection divided by that number, which for the examples of Figures 3-4, is 12:

$$\text{sim}(I_x, I_y) = |I_x \cap I_y| / 12$$

For the spatiotemporal examples of Figures 5-10, we use pixel overlap as the spatial measure for each frame, individually, but use only semi-quantitative estimation regarding the temporal aspects of the sequences, as described in the main text.

The model

The model’s architecture is described in detail in the main body, as is its algorithm, the code selection algorithm (CSA) including parameter values (Table 1) and so will not repeated here.

The learning law is Hebbian: simultaneous pre- and post-synaptic activation causes the synapse to be set to its max weight, 127, which is binary “1”. In the case of H and D weights, the weight is increased if the pre- and post-synaptic cells are active on successive time steps. In the full Sparsey model, additional learning properties are modeled including decay, permanence, and critical period, see (Rinkus 2014) for details. The simulations described in this paper are of small enough size, in terms of total numbers of inputs, which in the sequential case, means total number of frames (items) across all training sequences, so that these additional learning principles do not materially affect the results/conclusions.

Nevertheless, we briefly describe these additional principles. The overall goal of the decay protocol is that following an increase (which is always to the max weight), there is an initial period in which the weight remains at or near its max, and then an approximately exponential decay. This schedule works in concert with the permanence principle. The overall goal of permanence is that if a second pre-post coincidence occurs within a relatively small temporal window of the previous pre-post coincidence, then the weight will be made more resistant to decay, i.e., more permanent. In our simulations to date, these principles have been quantified in explicit tabular forms and rule-based use of the tables. The overall goal of the combined decay and permanence mechanism is to preferentially embed SDC codes of events that repeat, even once, within relatively small temporal windows. These also work in concert with a critical period mechanism. As we discussed, an SDC coding field has a finite storage capacity. The code space is exponential, e.g., in Sparsey’s case, K^Q , but as more and more codes are embedded in superposition, interference (crosstalk) accrues. As the fraction of the increased weights grows, expected retrieval accuracy falls and will go to zero if learning is not frozen, i.e., if a critical period is not enforced. In our full model, all three principles/mechanisms work in concert, but again, this paper’s simulations are small enough so that none of them come into play.

Code Similarity (Likelihood) Metric

Given that codes consist of one binary unit chosen from each of the Q competitive modules (CMs) comprising the coding field, code similarity is measured as Hamming distance normalized by code size, Q . Given: a) our assumption that input similarity correlates with likelihood; and b) that the model preserves input similarity into code similarity, we measure the likelihood (for either the spatial or spatiotemporal, i.e., “moment” case) of the stored (learned) input I_x given the current input I_c as:

$$L(I_x) = |\phi(I_c) \cap \phi(I_x)| / Q$$

Single Cell TF Images

The single cell surrogate TF images in Figure 12 were produced via a simple reverse correlation procedure. We took the set of images of the 6x6-binary pixel patterns occurring in the RF of a mac on all instances in which a particular cell in that mac is active and averaged them. This averaging was done using ImageJ's "Z-project" function, which computes the average intensity of each pixel across all images. The pixels are binary, so this process produces varying shades of gray as seen in the figure.

Acknowledgement

I'd like to thank the people who have encouraged me to pursue this theory over the years, including Dan Bullock, Jeff Hawkins, John Lisman, Josh Alspector, Tom McKenna, Andrew Browning, and Dan Hammerstrom. I'd also like to thank my colleagues at Neurithmic Systems, Greg Leshner, Jasmin Leveille, Oliver Layton, Harald Ruda, and Nick Nowak for their help developing these ideas. This work has been partially supported by DARPA contracts FA8650-13-C-7432 and N00173-09-C-2038, ONR contract N00014-12-C-0539, and NIH Training grant, 5 T32 NS07292.

References

- Abbott, L. F. and P. Dayan (1999). "The Effect of Correlated Variability on the Accuracy of a Population Code." Neural Computation **11**(1): 91-101.
- Ahmad, S. and J. Hawkins (2015). "Properties of Sparse Distributed Representations and their Application to Hierarchical Temporal Memory."
- Barlow, H. (1972). "Single units and sensation: a neuron doctrine for perceptual psychology? ." Perception **1**(4): 371 -394.
- Barth, A. L. and J. F. A. Poulet (2012). "Experimental evidence for sparse firing in the neocortex." Trends in Neurosciences **35**(6): 345-355.
- Bengio, Y. (2007). On the challenge of learning complex functions. Progress in Brain Research. T. D. Paul Cisek and F. K. John, Elsevier. **Volume 165**: 521-534.
- Bengio, Y., A. Courville and P. Vincent (2012). Representation Learning: A Review and New Perspectives, U. Montreal.
- Boerlin, M. and S. Denève (2011). "Spike-Based Population Coding and Working Memory." PLOS Computational Biology **7**(2): e1001080.
- Bogacz, R. (2007). "Optimal decision network with distributed representation." Neural Networks **20**(5): 564.
- Bonin, V., M. H. Histed, S. Yurgenson and R. C. Reid (2011). "Local Diversity and Fine-Scale Organization of Receptive Fields in Mouse Visual Cortex." The Journal of Neuroscience **31**(50): 18506-18521.
- Buzsáki, G. (2010). "Neural Syntax: Cell Assemblies, Synapsembles, and Readers." Neuron **68**(3): 362-385.
- Cox, D. D. and J. J. DiCarlo (2008). "Does Learned Shape Selectivity in Inferior Temporal Cortex Automatically Generalize Across Retinal Position?" J. Neurosci. **28**(40): 10045-10055.
- Cui, Y., S. Ahmad and J. Hawkins (2016). "Continuous online sequence learning with an unsupervised neural network model." Neural Computation **28**: 2474-2504.
- Curto, C., V. Itskov, K. Morrison, Z. Roth and J. L. Walker (2013). "Combinatorial Neural Codes from a Mathematical Coding Theory Perspective." Neural Comp **25**(7): 1891-1925.
- Deneve, S. and M. Chalk (2016). "Efficiency turns the table on neural encoding, decoding and noise." Current Opinion in Neurobiology **37**: 141-148.
- Doshi-Velez, F., D. Wingate, J. B. Tenenbaum and N. Roy (2011). Infinite Dynamic Bayesian Networks. 28th International Conference on Machine Learning, Bellevue, WA, USA.
- Franke, F., M. Fiscella, M. Sevelev, B. Roska, A. Hierlemann and R. Azere do da Silveira (2016). "Structures of Neural Correlation and How They Favor Coding." Neuron **89**(2): 409-422.
- Fries, P. (2009). "Neuronal Gamma-Band Synchronization as a Fundamental Process in Cortical Computation." Annual Review of Neuroscience **32**(1): 209-224.
- Fusi, S., E. K. Miller and M. Rigotti (2016). "Why neurons mix: high dimensionality for higher cognition." Current Opinion in Neurobiology **37**: 66-74.
- Georgopoulos, A., J. Kalaska, R. Caminiti and J. Massey (1982). "On the relations between the direction of two-dimensional arm movements and cell discharge in primate motor cortex." The Journal of Neuroscience **2**(11): 1527-1537.
- Grauman, K. and R. Fergus (2013). Learning Binary Hash Codes for Large-Scale Image Search. Machine Learning for Computer Vision. R. Cipolla, S. Battiato and G. M. Farinella. Berlin, Heidelberg, Springer Berlin Heidelberg: 49-87.
- Gripon, V., J. Heusel, M. Löwe and F. Vermet (2015). "A Comparative Study of Sparse Associative Memories."
- Hamel, Elizabeth J. O., Benjamin F. Grewe, Jones G. Parker and Mark J. Schnitzer (2015). "Cellular Level Brain Imaging in Behaving Mammals: An Engineering Approach." Neuron **86**(1): 140-159.
- Hebb, D. O. (1949). The organization of behavior; a neuropsychological theory. New York, Wiley.
- Hecht-Nielsen, R. (2007). Confabulation Theory: The Mechanism of Thought. Berlin, Springer-Verlag.
- Hochreiter, S. and J. Schmidhuber (1997). "Long short-term memory." Neural Computation **9**(8): 1735.

- Hubel, D. H. and T. N. Wiesel (1962). "Receptive fields, binocular interaction and functional architecture in the cat's visual cortex." J Physiol **160**: 106-154.
- Igarashi, K. M., L. Lu, L. L. Colgin, M.-B. Moser and E. I. Moser (2014). "Coordination of entorhinal-hippocampal ensemble activity during associative learning." Nature **510**(7503): 143-147.
- Jazayeri, M. and J. A. Movshon (2006). "Optimal representation of sensory information by neural populations." Nat Neurosci **9**(5): 690-696.
- Jercog, P., T. Rogerson and M. J. Schnitzer (2016). "Large-Scale Fluorescence Calcium-Imaging Methods for Studies of Long-Term Memory in Behaving Mammals." Cold Spring Harbor Perspectives in Biology **8**(5).
- Kanerva, P. (1988). Sparse distributed memory. Cambridge, MA, MIT Press.
- Kanerva, P. (2009). "Hyperdimensional Computing: An Introduction to Computing in Distributed Representation with High-Dimensional Random Vectors." Cognitive Computing **1**: 139-159.
- Kohn, A., R. Coen-Cagli, I. Kanitscheider and A. Pouget (2016). "Correlations and Neuronal Population Information." Annual Review of Neuroscience **39**(1): 237-256.
- Krizhevsky, A. and G. Hinton (2011). Using very deep autoencoders for content-based image retrieval. ESANN-2011, Bruges, Belgium.
- Latham, P. E. (2017). "Correlations demystified." Nat Neurosci **20**(1): 6-8.
- LeCun, Y., Y. Bengio and G. Hinton (2015). "Deep learning." Nature **521**(7553): 436-444.
- Ma, W. J., J. M. Beck, P. E. Latham and A. Pouget (2006). "Bayesian inference with probabilistic population codes." Nat Neurosci **9**(11): 1432-1438.
- Ma, W. J. and M. Jazayeri (2014). "Neural Coding of Uncertainty and Probability." Annual Review of Neuroscience **37**(1): 205-220.
- Mante, V., D. Sussillo, K. V. Shenoy and W. T. Newsome (2013). "Context-dependent computation by recurrent dynamics in prefrontal cortex." Nature **503**(7474): 78-84.
- Moreno-Bote, R., J. Beck, I. Kanitscheider, X. Pitkow, P. Latham and A. Pouget (2014). "Information-limiting correlations." Nat Neurosci **17**(10): 1410-1417.
- Nandy, Anirvan S., Jude F. Mitchell, Monika P. Jadi and John H. Reynolds (2016). "Neurons in Macaque Area V4 Are Tuned for Complex Spatio-Temporal Patterns." Neuron **91**(4): 920-930.
- Nandy, Anirvan S., Tatyana O. Sharpee, John H. Reynolds and Jude F. Mitchell (2013). "The Fine Structure of Shape Tuning in Area V4." Neuron **78**(6): 1102-1115.
- Pearl, J. (1988). Probabilistic Reasoning in Intelligent Systems: Networks of Plausible Inference San Mateo, CA, Morgan Kaufmann.
- Pitkow, X. and D. E. Angelaki (2016). "How the brain might work: Statistics flow in redundant population codes." (submitted).
- Poggio, T. and T. Serre. (2013). "Models of visual cortex." from http://www.scholarpedia.org/article/Models_of_visual_cortex.
- Pouget, A., J. M. Beck, W. J. Ma and P. E. Latham (2013). "Probabilistic brains: knowns and unknowns." Nat Neurosci **16**(9): 1170-1178.
- Pouget, A., P. Dayan and R. Zemel (2000). "Information processing with population codes." Nat Rev Neurosci **1**(2): 125-132.
- Pouget, A., P. Dayan and R. S. Zemel (2003). "Inference and Computation with Population Codes." Annual Review of Neuroscience **26**(1): 381-410.
- Rachkovskij, D. A. and E. M. Kussul (2001). "Binding and Normalization of Binary Sparse Distributed Representations by Context-Dependent Thinning." Neural Computation **13**(2): 411-452.
- Rajkumar, V. and X. Pitkow (2016). Inference by Reparameterization in Neural Population Codes.
- Riesenhuber, M. and T. Poggio (1999). "Hierarchical models of object recognition in cortex." Nat Neurosci **2**(11): 1019.
- Riesenhuber, M. and T. Poggio (2002). "Neural mechanisms of object recognition." Current Opinion in Neurobiology **12**(2): 162.
- Rinkus, G. (1996). A Combinatorial Neural Network Exhibiting Episodic and Semantic Memory Properties for Spatio-Temporal Patterns. Ph.D., Boston University.

- Rinkus, G. (2004). A Neural Model of Episodic and Semantic Spatiotemporal Memory. 26th Annual Conference of the Cognitive Science Society, Chicago, IL, Lawrence Erlbaum.
- Rinkus, G. (2008). Population Coding using Familiarity-Contingent Noise (poster). AREADNE 2008: Research in Encoding And Decoding of Neural Ensembles. Santorini, GR.
- Rinkus, G. (2012). "Quantum Computing via Sparse Distributed Representation." NeuroQuantology **10**(2): 311-315.
- Rinkus, G. (2013). A cortical theory of super-efficient probabilistic inference based on sparse distributed representations. CNS 2013, Paris.
- Rinkus, G. and J. Lisman (2005). Time-Invariant Recognition of Spatiotemporal Patterns in a Hierarchical Cortical Model with a Caudal-Rostral Persistence Gradient Society for Neuroscience Annual Meeting, Washington, DC.
- Rinkus, G. J. (2010). "A cortical sparse distributed coding model linking mini- and macrocolumn-scale functionality." Frontiers in Neuroanatomy **4**.
- Rinkus, G. J. (2014). "SparseyTM: Spatiotemporal Event Recognition via Deep Hierarchical Sparse Distributed Codes." Frontiers in Computational Neuroscience **8**.
- Rosenbaum, R., M. A. Smith, A. Kohn, J. E. Rubin and B. Doiron (2017). "The spatial structure of correlated neuronal variability." Nat Neurosci **20**(1): 107-114.
- Rust, N. C. and J. J. DiCarlo (2010). "Selectivity and Tolerance ("Invariance") Both Increase as Visual Information Propagates from Cortical Area V4 to IT." The Journal of Neuroscience **30**(39): 12978-12995.
- Salakhutdinov, R. and G. Hinton (2007). Semantic Hashing. SIGIR workshop on Information Retrieval and applications of Graphical Models.
- Salakhutdinov, R. and G. Hinton (2009). "Semantic hashing." International Journal of Approximate Reasoning **50**(7): 969-978.
- Sanger, T. D. (2003). "Neural population codes." Current Opinion in Neurobiology **13**(2): 238-249.
- Schneidman, E. (2016). "Towards the design principles of neural population codes." Current Opinion in Neurobiology **37**: 133-140.
- Schuldte, C., I. Laptev and B. Caputo (2004). Recognizing Human Actions: A Local SVM Approach. ICPR, Cambridge, UK.
- Serre, T., M. Kouh, C. Cadieu, U. Knoblich, G. Kreiman and T. Poggio (2005). A Theory of Object Recognition: Computations and Circuits in the Feedforward Path of the Ventral Stream in Primate Visual Cortex. AI Memo 2005-036, MIT.
- Shazeer, N., A. Mirhoseini, K. Maziarz, A. Davis, Q. Le, G. Hinton and J. Dean (2017) "Outrageously Large Neural Networks: The Sparsely-Gated Mixture-of-Experts Layer."
- Silver, D., A. Huang, C. J. Maddison, A. Guez, L. Sifre, G. van den Driessche, J. Schrittwieser, I. Antonoglou, V. Panneershelvam, M. Lanctot, S. Dieleman, D. Grewe, J. Nham, N. Kalchbrenner, I. Sutskever, T. Lillicrap, M. Leach, K. Kavukcuoglu, T. Graepel and D. Hassabis (2016). "Mastering the game of Go with deep neural networks and tree search." Nature **529**(7587): 484-489.
- Snaider, J. and S. Franklin (2011). Extended Sparse Distributed Memory. BICA.
- Snaider, J. and S. Franklin (2012). "Extended sparse distributed memory and sequence storage." Cognitive Computation **4**(2): 172-180.
- Snaider, J. and S. Franklin (2012). Integer Sparse Distributed Memory. FLAIRS Conference.
- Snaider, J. and S. Franklin (2014). "Modular composite representation." Cognitive Computation **6**(3): 510-527.
- Wang, J., W. Liu, S. Kumar and S. F. Chang (2016). "Learning to Hash for Indexing Big Data - A Survey." Proceedings of the IEEE **104**(1): 34-57.
- Watrous, A. J., J. Fell, A. D. Ekstrom and N. Axmacher (2015). "More than spikes: common oscillatory mechanisms for content specific neural representations during perception and memory." Current Opinion in Neurobiology **31**: 33-39.
- Willshaw, D. J., O. P. Buneman and H. C. Longuet-Higgins (1969). "Non Holographic Associative Memory." Nature **222**: 960-962.
- Yuste, R. (2015). "From the neuron doctrine to neural networks." Nat Rev Neurosci **16**(8): 487-497.

Zemel, R., P. Dayan and A. Pouget (1998). "Probabilistic interpretation of population codes." Neural Comput. **10**: 403-430.